

SEARCH FOR  $Z'$  VIA FORWARD BACKWARD ASYMMETRY IN DIELECTRON  
CHANNEL WITH THE CMS DETECTOR AT THE LARGE HADRON COLLIDER

A THESIS SUBMITTED TO  
THE GRADUATE SCHOOL OF NATURAL AND APPLIED SCIENCES  
OF  
MIDDLE EAST TECHNICAL UNIVERSITY

BY

MEHMET ÖZGÜR ŞAHİN

IN PARTIAL FULFILLMENT OF THE REQUIREMENTS  
FOR  
THE DEGREE OF MASTER OF SCIENCE  
IN  
PHYSICS

APRIL 2012

Approval of the thesis:

**SEARCH FOR Z' VIA FORWARD BACKWARD ASYMMETRY IN DIELECTRON  
CHANNEL WITH THE CMS DETECTOR AT THE LARGE HADRON COLLIDER**

submitted by **MEHMET ÖZGÜR ŞAHİN** in partial fulfillment of the requirements for the degree of **Master of Science in Physics Department, Middle East Technical University** by,

Prof. Dr. Canan Özgen  
Dean, Graduate School of **Natural and Applied Sciences**

\_\_\_\_\_

Prof. Dr. Mehmet T. Zeyrek  
Head of Department, **Physics**

\_\_\_\_\_

Prof. Dr. Meltem Serin  
Supervisor, **Physics Department**

\_\_\_\_\_

Prof. Dr. Mehmet T. Zeyrek  
Co-supervisor, **Physics Department**

\_\_\_\_\_

**Examining Committee Members:**

Prof. Dr. Namık Kemal Pak  
Physics Department, METU

\_\_\_\_\_

Prof. Dr. Meltem Serin  
Physics Department, METU

\_\_\_\_\_

Prof. Dr. Müge Boz Evinay  
Physics Engineering Department, Hacettepe University

\_\_\_\_\_

Dr. Sezen Sekmen  
CERN

\_\_\_\_\_

Prof. Dr. Ali Ulvi Yilmazer  
Physics Engineering Department, Ankara University

\_\_\_\_\_

**Date:**

\_\_\_\_\_

**I hereby declare that all information in this document has been obtained and presented in accordance with academic rules and ethical conduct. I also declare that, as required by these rules and conduct, I have fully cited and referenced all material and results that are not original to this work.**

Name, Last Name: MEHMET ÖZGÜR ŞAHİN

Signature :

## ABSTRACT

SEARCH FOR  $Z'$  VIA FORWARD BACKWARD ASYMMETRY IN DIELECTRON CHANNEL WITH THE CMS DETECTOR AT THE LARGE HADRON COLLIDER

Şahin, Mehmet Özgür

M.Sc., Department of Physics

Supervisor : Prof. Dr. Meltem Serin

Co-Supervisor : Prof. Dr. Mehmet T. Zeyrek

April 2012, 43 pages

In this thesis, analysis of the forward backward asymmetry of high energy electron pairs at the CMS - LHC with a centre of mass energy of 7 TeV is presented and the possibility of search for a new neutral weak boson  $Z'$  via measuring the forward backward asymmetry  $A_{FB}$  of high energy electron pairs is discussed. The forward backward asymmetry is a natural result of the interference between the neutral current mediators: Photon and Z boson. A new neutral gauge boson would also interfere with these mediators and this new interference would either enhance the forward backward asymmetry at high energies or suppress it. In this analysis,  $4.67 \text{ fb}^{-1}$  data collected at the CMS experiment in 2011 is used.

Keywords: Forward Backward Asymmetry,  $Z'$  boson, LHC, CMS, Dielectron

## ÖZ

### BÜYÜK HADRON ÇARPIŞTIRICISININ CMS DETEKTÖRÜNDE İLERİ GERİ ASİMETRİSİ KULLANILARAK DİELEKTRON KANALINDA Z' BOZONLARININ ARAŞTIRILMASI

Şahin, Mehmet Özgür

Yüksek Lisans, Fizik Bölümü

Tez Yöneticisi : Prof. Dr. Meltem Serin

Ortak Tez Yöneticisi : Prof. Dr. Mehmet T. Zeyrek

Nisan 2012, 43 sayfa

Bu tezde, 7 TeV kütle merkezi enerjili CMS - LHC deneyindeki yüksek enerjili dielektronların ileri geri asimetrisinin analizi ve bu asimetri kullanılarak yeni bir nötr zayıf bozon olan Z' parçacığının aranışı ihtimali tartışılmıştır. İleri geri asimetrisi, yüksüz akımları ileten foton ve Z bozonu girişiminin doğal bir sonucudur. Yeni bir yüksüz ayar bozonunda bu parçacıklarla girişim yapar ve ileri geri asimetrisini güçlendirir veya azaltır. Bu analizde, 2011 yılında CMS detektöründe toplanan  $4.67 \text{ fb}^{-1}$  büyüklüğündeki data kullanılmıştır.

Anahtar Kelimeler: İleri Geri Asimetrisi, Z' Bozonu, BHÇ, CMS, Dielektron

*...to my family, Sezoş and friends who supported me along the way.*

## ACKNOWLEDGMENTS

I owe my most sincere thanks to my supervisor, Prof. Dr. Meltem Serin. She provided me encouragement and support in every aspect of my work. The good advice and support of my co-supervisor, Prof. Dr. Mehmet T. Zeyrek, have been invaluable on both an academic and a personal level, for which I am sincerely grateful.

This thesis would not have been possible without the patience and support of Dr. Efe Yazgan, who gave me the opportunity to work with him at CERN and gave me limitless help during my difficult moments. He guided me in every step of my analysis. I would like to acknowledge Dr. Sezen Sekmen not only for sharing her great knowledge on experimental physics, but also sharing her vision and showing me the world in a way that I have never been able to see it before.

I wish to express sincere gratitude to Prof. Dr. Namık Kemal Pak, his broad experience and understanding have had a remarkable influence on my entire life. It was a great pleasure for me to be his student.

I wish to thank Buğra Bilin for the beneficial discussions, his friendship and for his precious collaboration at CERN. Also during my days at METU, I have been blessed with cheerful friendship of my colleagues Enis Doko, Selçuk Bilmiş and Uğur E. Surat.

I owe my loving thanks to my love Seza Göker. She enlightened my way and helped me to overcome even the most desperate moments. My warm thanks are due to Anıl Kavaz, Duygu Tekin, Anıl Ekici and especially Caner Uzun, for their great support and friendship since the beginning of our high school years.

Last but not least, I owe deepest gratitude to my family for their loving support for which my mere expression of thanks does not suffice. Without their encouragement and understanding, it would have been impossible for me to finish this work.

# TABLE OF CONTENTS

ABSTRACT . . . . .	iv
ÖZ . . . . .	v
ACKNOWLEDGMENTS . . . . .	vii
TABLE OF CONTENTS . . . . .	viii
LIST OF TABLES . . . . .	x
LIST OF FIGURES . . . . .	xi
CHAPTERS	
1 INTRODUCTION . . . . .	1
2 THEORY . . . . .	3
2.1 Standard Model . . . . .	3
2.2 Electroweak Interactions . . . . .	4
2.3 Forward Backward Asymmetry . . . . .	5
2.3.1 $Z'$ Particle . . . . .	8
2.3.1.1 Effective $U(1)_{Y'}$ Model . . . . .	10
2.3.1.2 L-R Symmetric Model . . . . .	10
2.3.1.3 Sequential Standard Model . . . . .	11
3 THE LARGE HADRON COLLIDER AND THE COMPACT MUON SOLENOID DETECTOR . . . . .	12
3.1 The Large Hadron Collider . . . . .	12
3.2 The Compact Muon Solenoid Detector . . . . .	15
3.2.1 Inner Tracking System . . . . .	17
3.2.2 Electromagnetic Calorimeter (ECAL) . . . . .	17
3.2.2.1 Photodetectors . . . . .	18
3.2.2.2 Preshower . . . . .	18

3.2.3	Hadron Calorimeter . . . . .	18
3.2.4	Forward Detectors . . . . .	19
3.2.5	The Muon System . . . . .	19
3.2.6	Trigger and Data Acquisition . . . . .	20
3.2.6.1	Level-1 Trigger . . . . .	20
3.2.6.2	High Level Trigger and Data Acquisition . . . . .	22
3.2.7	Computing . . . . .	22
3.2.7.1	Offline Computing . . . . .	22
4	DATA SELECTION AND MONTE CARLO SAMPLES . . . . .	24
4.1	Data Selection and Monte Carlo Samples . . . . .	24
4.2	Electron Reconstruction . . . . .	25
4.3	Z Boson Reconstruction . . . . .	28
5	ANALYSIS OF FORWARD BACKWARD ASYMMETRY . . . . .	32
5.1	Scattering Angle Distributions in the Collins Soper Frame . . . . .	32
5.2	Forward Backward Asymmetry . . . . .	35
6	CONCLUSION . . . . .	40
	REFERENCES . . . . .	42

# LIST OF TABLES

## TABLES

Table 2.1	Couplings of Neutral Currents . . . . .	6
Table 4.1	Triggers and Corresponding run numbers used in $A_{FB} - Z'$ analysis . . . . .	24
Table 4.2	MC Samples for SM and the corresponding cross sections. . . . .	25
Table 4.3	HEEP Selection Criteria: While first two variables stand for kinematic and geometric properties, second set stands for identification (ID) cuts and third set for the isolation cuts. . . . .	28
Table 4.4	Fraction of particles that pass through HEEP Selection Criteria in percentage. Here the column headers give the name of corresponding data and MC samples. . . . .	29

# LIST OF FIGURES

## FIGURES

Figure 2.1 Elementary particles of the Standard Model . . . . .	4
Figure 2.2 First order Feynman diagrams of $q\bar{q} \rightarrow e^-e^+$ neutral currents in the Standard Model . . . . .	5
Figure 2.3 First order Feynman diagram for the process $q\bar{q} \rightarrow Z^0/Z'/\gamma \rightarrow e^-e^+$ . . . . .	8
Figure 2.4 First order Feynman diagram for the process $q\bar{q} \rightarrow Z^0/Z'/\gamma \rightarrow e^-e^+$ . . . . .	8
Figure 2.5 Comparison of Invariant Mass for different $Z'$ models [6] . . . . .	9
Figure 2.6 Comparison of $A_{FB}$ for different $Z'$ models [6] . . . . .	10
Figure 3.1 Geographical Location of the LHC [12] . . . . .	12
Figure 3.2 The LHC Schematic [14] . . . . .	13
Figure 3.3 Structural view of a LHC Dipole [15] . . . . .	14
Figure 3.4 An overview of the CMS Detector [2] . . . . .	15
Figure 3.5 Layered Structure of CMS: Transverse Slice [22] . . . . .	16
Figure 3.6 Layered Structure of CMS: Longitudinal Slice [24] . . . . .	17
Figure 3.7 Overview of ECAL detector [26] . . . . .	18
Figure 3.8 Triggering structure of the CMS experiment [2] . . . . .	21
Figure 4.1 GSF Electron interaction with the detector . . . . .	26
Figure 4.2 Energy distribution of opposite charged dielectron pairs . . . . .	29
Figure 4.3 Pseudo rapidity distribution of oppositely charged dielectron pairs . . . . .	30
Figure 4.4 Pseudo rapidity distribution of reconstructed Z bosons . . . . .	30
Figure 4.5 Invariant Mass histogram in range: 0.06-1.4 TeV . . . . .	31

Figure 5.1 $\cos \theta_{CS}^*$ distribution within an invariant mass interval of $60\text{GeV} < \sqrt{s} < 300\text{GeV}$ . . . . .	33
Figure 5.2 $\cos \theta_{CS}^*$ distribution within an invariant mass interval of $400\text{GeV} < \sqrt{s} < 1400\text{GeV}$ . . . . .	34
Figure 5.3 Forward Backward Asymmetry within the range $2.5 >  Y  > 0.8$ and $60\text{GeV} < \sqrt{s} < 1400\text{GeV}$ . . . . .	36
Figure 5.4 Forward Backward Asymmetry within the range $0.8 >  Y $ and $60\text{GeV} < \sqrt{s} < 1400\text{GeV}$ . . . . .	36
Figure 5.5 Forward Backward Asymmetry within the range $2.1 >  Y  > 0.8$ and $60\text{GeV} < \sqrt{s} < 1400\text{GeV}$ . . . . .	37
Figure 5.6 Forward Backward Asymmetry within the range $60\text{GeV} < \sqrt{s} < 1400\text{GeV}$	39

# CHAPTER 1

## INTRODUCTION

The Large Hadron Collider (LHC) [1] is a high energy hadron collider that has been operating and providing collisions for the detectors since 2009. The Compact Muon Solenoid (CMS) [2] is a general purpose detector, as one of the four main detectors placed at the LHC, collected more than  $4.7 \text{ fb}^{-1}$  data from proton collisions with 7 TeV (by 2012 8 TeV) center of mass energy since 2010. It aims to explore the TeV scale physics at the LHC.

The Standard Model (SM) is a  $SU(3)_C \times SU(2)_L \times U(1)_Y$  gauge symmetric model describing the interactions between the fundamental building blocks of matter, i.e. quarks and leptons. Although it describes subatomic world with a great precision, due to the questions it left unanswered, SM is not accepted as the ultimate theory but more of a main step forward to it. However, without the guidance of experimental evidence, such an ultimate theory can not be constructed. Therefore, search for the *new physics* or physics beyond the Standard Model is one of the main purposes of the research activities at the LHC, in general, and the CMS experiment.

Forward backward asymmetry was first proposed by Zel'dovich [3] to understand the nature of the weak interactions at the low energies. The reason to observe such an asymmetry is the interference between photons and Z bosons which are the neutral current mediators, and the left right asymmetric couplings of the weak interactions. A new neutral boson is proposed in the context of a Beyond the Standard Model also interferes with these bosons and therefore affects the forward backward asymmetry. Hence, by understanding the true nature of the forward backward asymmetry, existence of these particles can be checked.

In this thesis, the forward backward asymmetry for high energy dielectrons at the CMS experiment will be presented and possibility of searches for the new neutral bosons will be discussed. In the next chapter, the theoretical background for the analysis will be given. In the chapter 3, a general scheme of the LHC and the CMS experiment will be presented, and then the event reconstruction and the data selection will be discussed. The analysis of forward backward asymmetry will be presented in chapter five and results will be discussed in the last chapter.

## CHAPTER 2

### THEORY

#### 2.1 Standard Model

Standard Model is a  $SU(3)_C \times SU(2)_L \times U(1)_Y$  gauge symmetric model which describes the elementary particles and their interactions. These interactions include Electromagnetic Interactions, Weak Interactions and Strong Interactions. The Standard Model interactions are mediated by bosons.

There are 3 lepton and quark families in the Standard Model. Minimum number of quark families is set by the CKM (Cabibbo Kobayashi Maskawa) matrix in order to include Charge Parity violation into quark mixing. On the other hand, only restriction in the number of lepton generations comes from experimental measurements of ratio of the Z boson's decay width into invisible modes (neutrinos) that allows only three light neutrino flavors:

$$\frac{\Gamma_{invs}}{\Gamma_l} = \frac{N_\nu \Gamma(Z \rightarrow \bar{\nu}\nu)}{\Gamma_l} \sim 2N_\nu \quad (2.1)$$

Measured value of  $\Gamma_{invs}/\Gamma_l$  is  $5.942 \pm 0.016$  [4]. However a fourth neutrino with mass greater than  $m_{Z^0}/2$  might possibly exist. Quarks have an additional quantum number that is called color and color number can be experimentally obtained from the ratio:

$$R_{e^+e^-} = \frac{\sigma(e^+e^- \rightarrow hadrons)}{\sigma(e^+e^- \rightarrow \mu^+\mu^-)}. \quad (2.2)$$

With three different color charges (Red, blue, green), quarks form a  $SU(3)$  color group where three colors are the fundamental representatives of this group. This local gauge symmetry dictates interactions between the color charged quarks and the interaction is named as Quantum Chromo Dynamics (QCD) and mediated by (also color charged) gluons. Gluons also have color charge; therefore, unlike photons, self interaction is possible for gluons.

	2.4 MeV $\frac{2}{3}$ $\frac{1}{2}$ <b>u</b> up	1.27 GeV $\frac{2}{3}$ $\frac{1}{2}$ <b>c</b> charm	171.2 GeV $\frac{2}{3}$ $\frac{1}{2}$ <b>t</b> top	0 0 1 <b><math>\gamma</math></b> photon
Quarks	4.8 MeV $-\frac{1}{3}$ $\frac{1}{2}$ <b>d</b> down	104 MeV $-\frac{1}{3}$ $\frac{1}{2}$ <b>s</b> strange	4.2 GeV $-\frac{1}{3}$ $\frac{1}{2}$ <b>b</b> bottom	0 0 1 <b>g</b> gluon
	<2.2 eV 0 $\frac{1}{2}$ <b><math>\nu_e</math></b> electron neutrino	<0.17 MeV 0 $\frac{1}{2}$ <b><math>\nu_\mu</math></b> muon neutrino	<15.5 MeV 0 $\frac{1}{2}$ <b><math>\nu_\tau</math></b> tau neutrino	91.2 GeV 0 1 <b><math>Z^0</math></b> weak force
Leptons	0.511 MeV -1 $\frac{1}{2}$ <b>e</b> electron	105.7 MeV -1 $\frac{1}{2}$ <b><math>\mu</math></b> muon	1.777 GeV -1 $\frac{1}{2}$ <b><math>\tau</math></b> tau	80.4 GeV $\pm 1$ 1 <b><math>W^\pm</math></b> weak force
				Bosons (Forces)

Figure 2.1: Elementary particles of the Standard Model

## 2.2 Electroweak Interactions

Unification of electromagnetic and weak interactions is the most encouraging step towards the grand unified theories. To construct such a unified theory required experimental evidences. From the results deduced from the experiments, only left handed particles and right handed anti particles interact via weak interactions. Therefore, weak interactions' mediator bosons,  $Z^0$  and  $W^{+,-}$ , only couple to the left handed particle doublets. On the other hand, photons interact with both right handed and left handed particles. Moreover, unlike photons,  $Z^0$  and  $W^{+,-}$  bosons are massive particles and their masses are in the range of 80 GeV to 100 GeV. However, massive bosons are forbidden by Gauge Symmetry. The problem is solved adequately by Spontaneous Symmetry Breaking mechanism through the Higgs field and Higgs particles.

The simplest unitary group that includes doublets is  $SU(2)$ . Global gauge transformations that leave weak interaction invariant in flavor space also introduce  $U(1)_Y$  instead of simple  $U(1)_Q$

group of Quantum Electrodynamics where Y (hypercharge) is defined as

$$Y = Q - T_3 \quad (2.3)$$

Here  $T_3 = \sigma_3/2$  and Q stands for the electromagnetic charge operator. All in all, the Electroweak theory eventually becomes a unified  $SU(2)_L \times U(1)_Y$  gauge symmetric theory.

### 2.3 Forward Backward Asymmetry

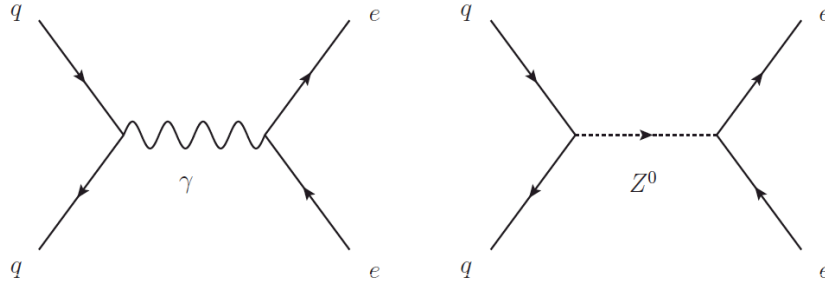


Figure 2.2: First order Feynman diagrams of  $q\bar{q} \rightarrow e^-e^+$  neutral currents in the Standard Model

Since 1960's Forward Backward Asymmetry ( $A_{FB}$ ) has been considered as a useful tool initially for the first observations of Neutral Currents (NC) and then to make precision measurements of NC. Due to the unified nature of Weak interactions and QED, Lagrangian of NC can be written in the form of

$$\mathcal{L}_N = \mathcal{L}_{QED} + \mathcal{L}_N^Z \quad (2.4)$$

with QED Lagrangian

$$\mathcal{L}_{QED} = -eA_\mu \sum \bar{f}\gamma^\mu q_f f \quad (2.5)$$

and Neutral Z Current Lagrangian

$$\mathcal{L}_N^Z = -\frac{e}{2 \sin \theta_W \cos \theta_W} Z_\mu \sum \bar{f}\gamma^\mu (v_f - a_f \gamma_5) f \quad (2.6)$$

Table 2.1: Couplings of Neutral Currents

	$u, c, t$	$d, s, b$	$e, \mu, \tau$
$v_f$	$\frac{1}{2} - \frac{4}{3} \sin^2 \theta_W$	$-\frac{1}{2} + \frac{2}{3} \sin^2 \theta_W$	$-\frac{1}{2} + 2 \sin^2 \theta_W$
$a_f$	$\frac{1}{2}$	$-\frac{1}{2}$	$-\frac{1}{2}$

and the coupling constants of neutral currents given in table 2.1

As it can be seen from the Lagrangian,  $f\bar{f} \rightarrow \bar{l}l$  interaction is mediated by both  $\gamma$  and  $Z$  boson and the asymmetry arises as a result of their interference. With the appropriate coupling constants, one can calculate the following differential cross section for the interaction  $f\bar{f} \rightarrow Z/\gamma \rightarrow \bar{l}l$

$$\frac{d\sigma}{d\Omega} \sim A_0(1 + \cos^2 \theta) + A_1 \cos \theta \quad (2.7)$$

Here the last term is the real source of asymmetry since it gives non zero terms for the difference of forward and backward hemispheres. Writing

$$F = \int_0^1 \frac{d\sigma}{d(\cos \theta)} d(\cos \theta) \quad \text{and} \quad B = \int_{-1}^0 \frac{d\sigma}{d(\cos \theta)} d(\cos \theta) \quad (2.8)$$

$A_{FB}$  can be defined as

$$A_{FB} = \frac{F - B}{F + B} = \frac{3A_1}{8A_0} \quad (2.9)$$

where  $F$  stands for particles going in forward region and conventionally chosen as the direction of *matter* (here *matter* describes opposite of anti matter) whereas  $B$  stands for particles going in backward direction and conventionally chosen as direction of *anti-matter*. Forward Backward Asymmetry arises due to fact that  $Z$  boson couples to left and right handed particles differently. Defining  $c_L = v_f - a_f$  and  $c_R = v_f + a_f$  as the left handed and right handed couplings,  $A_0$ 's and  $A_1$ 's dependencies on these couplings can be discussed. Apparently, asymmetry arises from the  $c_L - c_R$  factors that appears in the  $A_1$  parameter and all the terms have a dependency on the propagator of the  $Z$  boson  $r \sim \frac{s}{s - M_Z^2 + iM_Z\Gamma_Z}$  except the constant (constant with respect to  $r$ ) term coming from Quantum Electro Dynamics. At low energies

( $< M_Z$ ),  $A_0$  is dominated by the constant term since  $r$  is very small and  $A_1$  gives a small negative value since  $s < M_Z$ . At very low energies however, the only surviving term will be the constant term in  $A_0$  hence the  $A_{FB} = 0$ . Therefore, setting  $A_1 \rightarrow 0$  and  $A_0 \rightarrow 1$  gives us the pure QED case for which weak interactions are the main source of  $A_{FB}$ . At the energies close to the Z peak ( $\sim 90$  GeV)  $A_1$  goes to zero and takes high values due to the finite width of Z in the propagator. Therefore, around Z peak  $A_{FB}$  approaches 0. Finally, for high energies  $s$  dominates both  $A_0$  and  $A_1$  and gives a constant  $A_{FB}$  ( $\sim 0.6$ ) directly related with  $c_L$  and  $c_R$ . Unfortunately, the picture given above has to be modified to discuss quark anti quark interactions which have to be confined to a hadron and there is no anti particle beam at the LHC; therefore, all the anti-matter in collisions are coming from the sea quarks and matter mostly coming from the valance quarks inside of partons. Sea quarks are responsible for very small amount of mass and energy of protons. As a result, valance quarks are boosted and their directions are chosen as forward direction. Further, even if quarks collide head on, direction of the collision may differ from the incident beams' directions ( $q\bar{q}$  problem). This effect can be related to mainly three different phenomena. At low energies ( $< 10$  GeV) bremsstrahlung photons coming from the proton may create a new lepton pair; moreover, internal quark interactions may result with a boost in transverse direction due to the compositeness of the protons [5]. At high energies, on the other hand, most of the quarks' momenta are distributed in beam direction ( $p_z$ ). However, with hard photon and gluon emission, quarks can gain a boost in the transverse direction as pictured in figure 2.3.

The boost in the transverse direction changes the center of mass frame of the quark anti quark interactions so that it differs from the protons' center of mass frame. Therefore, we use the Collins Soper frame [5] which is the best approximation to the CM frame of quark interactions. The scattering angle in the Collins Soper frame can be written as

$$\cos \theta_{CS}^* = \frac{2(P_1^+ P_2^- - P_1^- P_2^+)}{\sqrt{Q^2(Q^2 + Q_T^2)}} \quad (2.10)$$

where  $Q$  and  $Q_T$  are the four-momentum and the transverse momentum of the di-lepton system,  $P_{1,2}$  represent the four-momentum components of  $l$  and  $\bar{l}$ , and  $P_i^\pm = \frac{1}{\sqrt{2}}(P_i^0 \pm P_i^3)$ . Now the effect of the boost can be applied

$$\cos \theta_{CS}^* \rightarrow \frac{P_z(\bar{l})}{|P_z(\bar{l})|} \cos \theta_{CS}^* \quad (2.11)$$

Without hard emission of photons and gluons,  $\cos \theta_{CS}^*$  is reduced to  $\cos \theta^*$ , that is to say for the leading order, the Collins Soper frame approximation is not necessary. Another approach

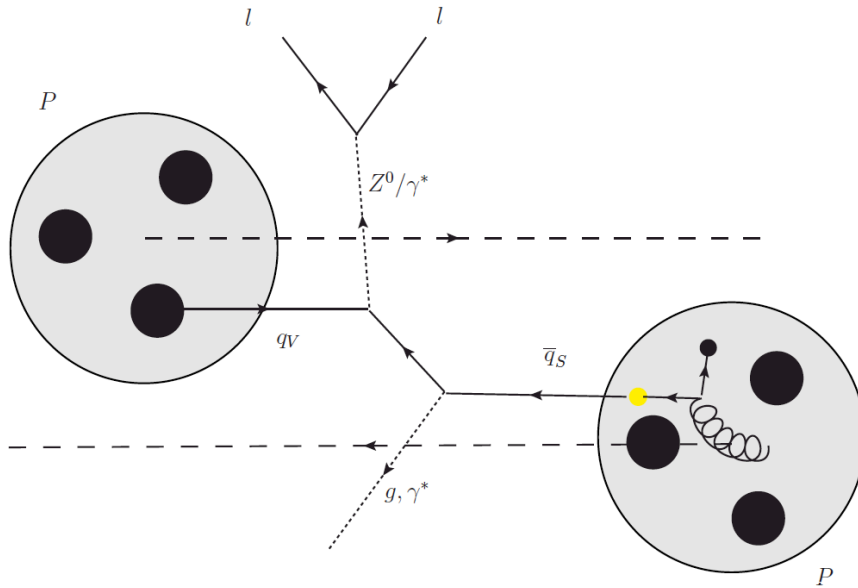


Figure 2.3: First order Feynman diagram for the process  $q\bar{q} \rightarrow Z^0/Z'/\gamma \rightarrow e^-e^+$

is to apply rapidity cut ( $Y > 0.8$ ) on the leptons so that the resulting leptons are very close to the initial direction of the beam [6]. These leptons are most likely the result of the collision of quarks and these quarks' center of mass reference frame very close to center of mass frame of the protons.

### 2.3.1 $Z'$ Particle

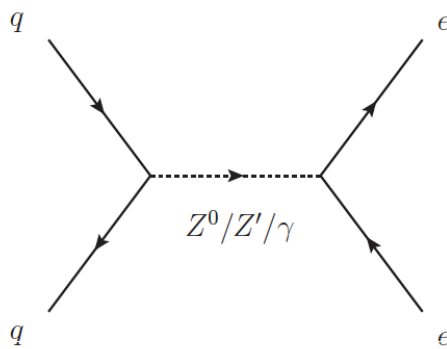


Figure 2.4: First order Feynman diagram for the process  $q\bar{q} \rightarrow Z^0/Z'/\gamma \rightarrow e^-e^+$

Forward backward asymmetry can also be a useful tool for the discovery of heavy neutral

gauge bosons ( $Z'$ ) which are proposed by many Beyond the Standard Model theories ([7]-[11]) such as *MSSM*, *E6*, *SSM*, *LR symmetric models*, etc. As it is discussed earlier, near the  $Z$ -peak the asymmetry goes to zero, since in that region the interaction is mostly dominated by the  $Z$  boson itself, same behavior of asymmetry should also be observed for a possible extra neutral gauge boson scenario. Off the peak, above  $Z'$  mass, each model contributes (alters)  $A_{FB}$  according to its couplings. Hence, though not the best method (again for the statistical reasons, mass resonances hunting is the best method), analyzing  $A_{FB}$  is an alternate way to search for Heavy Neutral Gauge bosons, and in terms of distinguishing between different models  $A_{FB}$  has great advantage over other methods since it is very sensitive for different couplings as it can be seen from figures 2.5 and 2.6 [7]. Hence, it is also sensitive to broad resonances that can be missed by invariant mass analysis. Moreover, since BSM couplings are directly related to  $\sin^2 \theta_W$ ,  $A_{FB}$  provides a precise measurement opportunity for the BSM  $\sin^2 \theta_W$ .

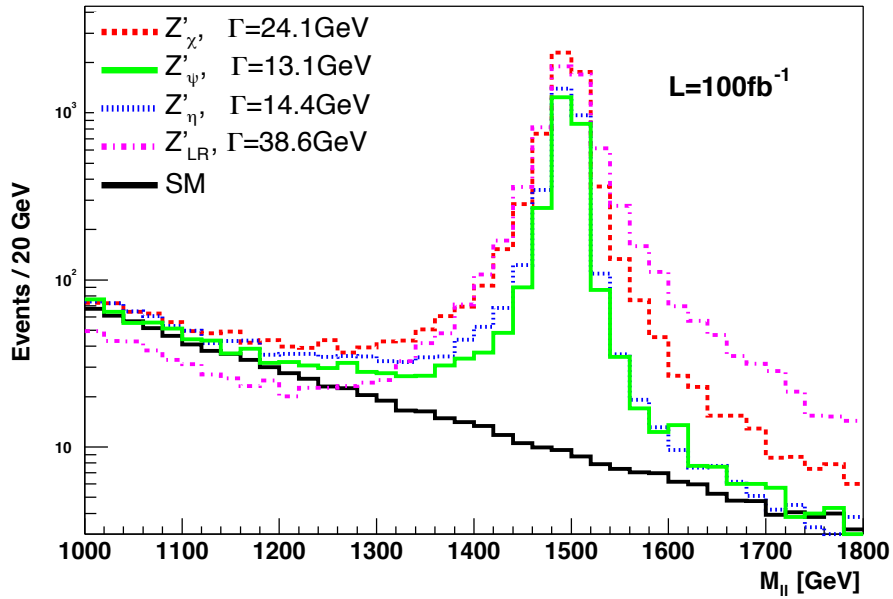


Figure 2.5: Comparison of Invariant Mass for different  $Z'$  models [6]

Some Beyond the Standard Model scenarios (a review of the complete list of these models could be a new thesis topic by itself; therefore, we will only deal with the well motivated E6 decomposition models, and in addition to two E6 models, as the simplest case, Sequential

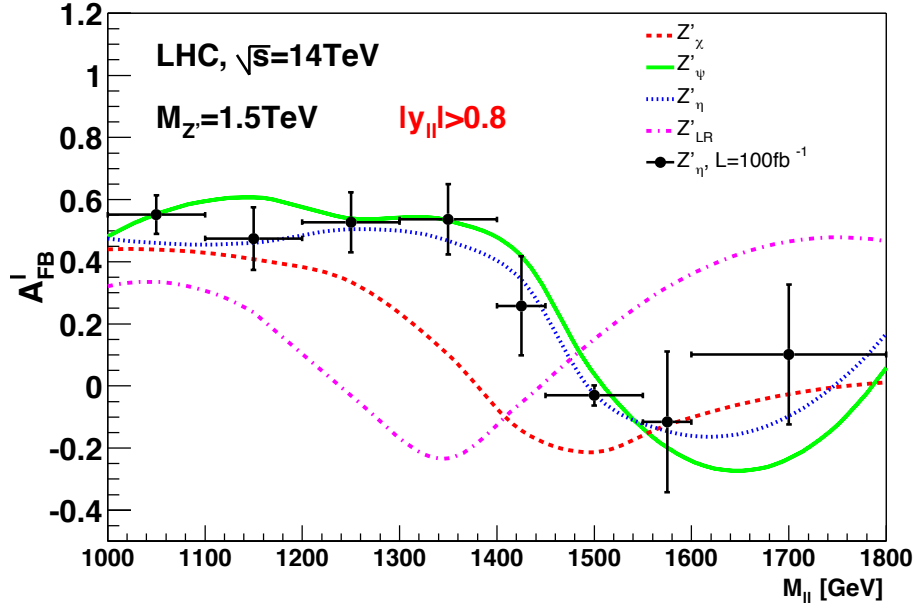


Figure 2.6: Comparison of  $A_{FB}^I$  for different  $Z'$  models [6]

Standard Model) that predicts  $Z'$  particles in the TeV scale is listed in [6]:

### 2.3.1.1 Effective $U(1)_{Y'}$ Model

This model is a result of the following breaking chain that is favored by most of the Grand Unified Theories.

$$E_6 \rightarrow SO(10) \times U(1)_\psi \rightarrow SU(5) \times U(1)_\psi \times U(1)_\chi \rightarrow SU(3)_C \times SU(2)_L \times U(1)_Y \times U(1)_{Y'} \quad (2.12)$$

This breaking results in with two different hypercharge states and  $Z'$  can be parametrized in terms of these hypercharges as

$$Z' = Z'_\chi \cos \beta + Z'_\psi \sin \beta \quad (2.13)$$

### 2.3.1.2 L-R Symmetric Model

This model, with more than 4 versions, restores Left Right symmetry at high energies with a heavy  $Z'$ . Therefore, an additional  $SU(2)_L$  term is required and this term leads LR couplings

in addition to the SM couplings.

### **2.3.1.3 Sequential Standard Model**

The Sequential Standard Model is actually the Standard Model itself with an additional heavy neutral boson. The Sequential Standard Model is not gauge invariant; therefore, it is not realistic and favorable in terms of theoretical physics point of view. On the other hand, it is very useful for comparison purposes since it has same coupling constants with the Standard Model and  $Z'$  samples that are generated in the Sequential Standard Model are used in this thesis.

## CHAPTER 3

# THE LARGE HADRON COLLIDER AND THE COMPACT MUON SOLENOID DETECTOR

### 3.1 The Large Hadron Collider

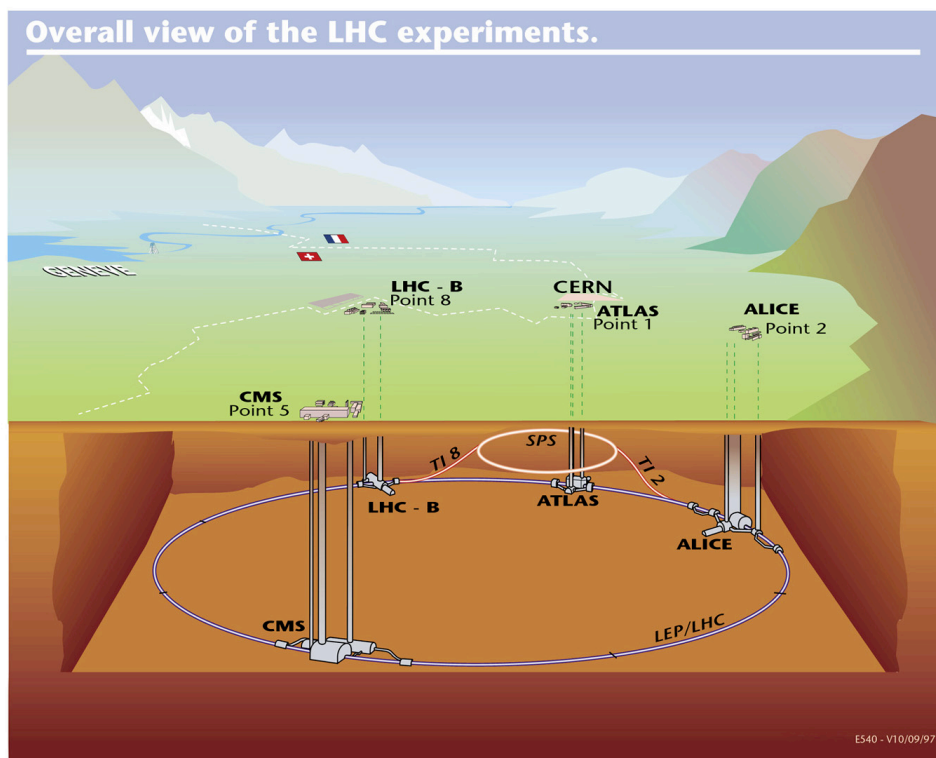


Figure 3.1: Geographical Location of the LHC [12]

The Large Hadron Collider (LHC) [1] is a hadron accelerator and collider that placed in a 26.7 km circumference circular tunnel which straddles the French and Swiss borders (figure

3.1) and buried underground between a a depth of 45 m to 175 m from the surface. Due to the necessity to investigate Electroweak Symmetry Breaking and other interesting High Energy Physics phenomena like scalar TeV scale dark matter candidates, the LHC is designed to collide protons with a center of mass energy of 14 TeV and a luminosity of  $10^{34} \text{ cm}^{-2}\text{s}^{-1}$  since only with this high luminosity and energy, the rare events proposed by these new physics phenomena can be explored and maybe discovered. The LHC is also capable of colliding lead beams (Pb) with a maximum luminosity  $10^{27} \text{ cm}^{-2}\text{s}^{-1}$  and an energy 2.8 TeV per nucleon. The center of mass energy that is provided by the LHC is 6 times more than its predecessor Tevatron, and the LHC has 30 times larger design luminosity [13]. These advantages makes LHC the most powerful tool to explore TeV scale physics and explore possible TeV scale Beyond the Standard Model scenarios.

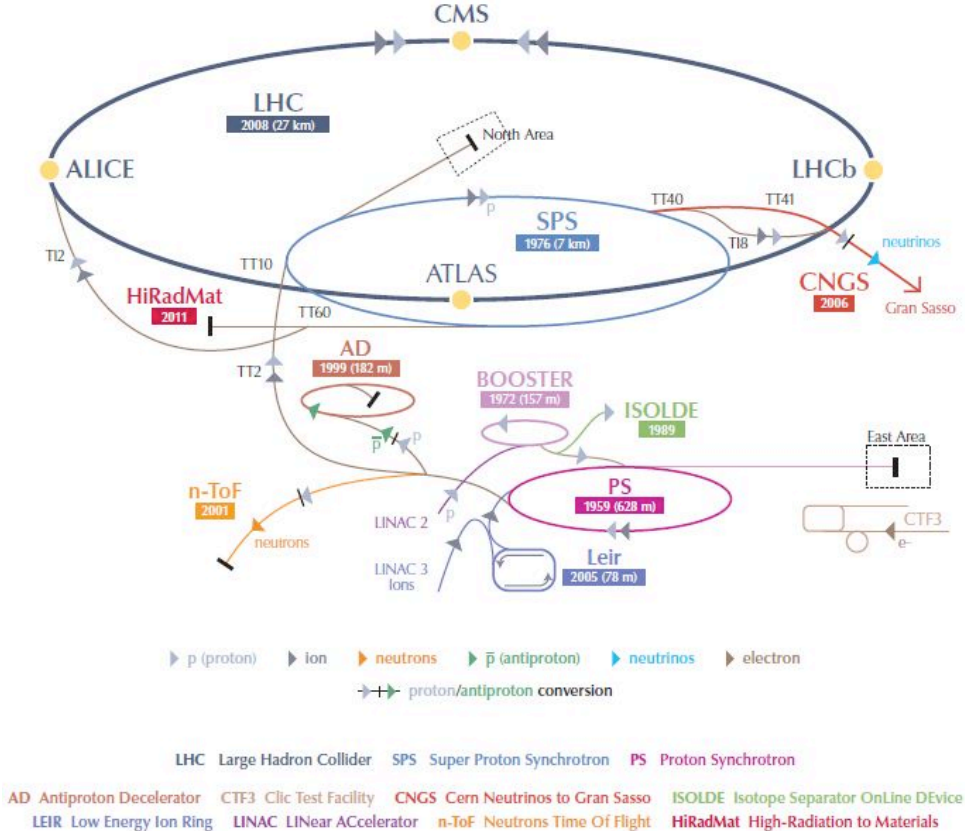


Figure 3.2: The LHC Schematic [14]

There are more than ~1500 magnets with various types placed inside of old LEP tunnel in

order to reach the indicated specifications. In order to bend 7 TeV proton beams a magnetic field of  $\sim 8.33$  Tesla is required and that is obtained by NbTi superconductors cooled down below  $\sim 1.9$  K. The bending is mainly done by 1232 dipoles, and more than  $\sim 300$  quadrupoles are used for focusing. To reduce cost and reach maximum performance within the space limitations, two in one design is applied to almost all magnets, so two opposite direction beam channels benefit from the same cold mass and opposite magnetic flux.

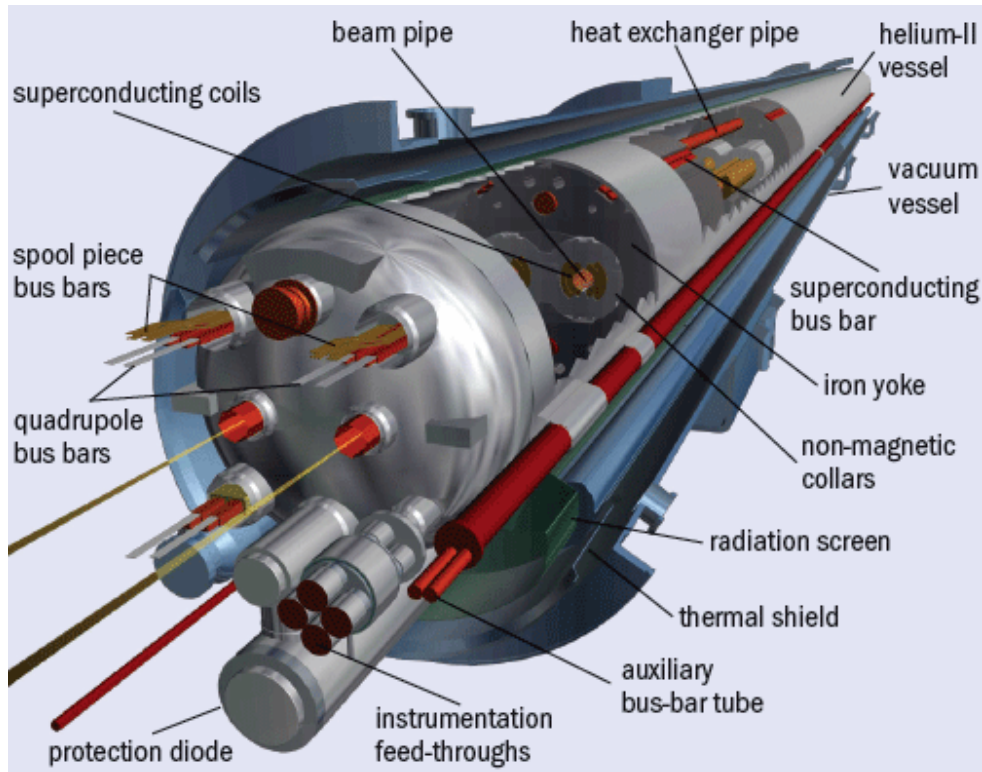


Figure 3.3: Structural view of a LHC Dipole [15]

Proton beams at the LHC are generated by Linac2 and follow Proton Synchrotron Booster (PSB) - Proton Synchrotron (PS) - Super Proton Synchrotron (SPS) path and enter LHC ring with 450 GeV energy and then inside of LHC can be accelerated up to 7 TeV. Finally, after two beams are accelerated in opposite directions, they collide inside the four main experiments (detectors) at the LHC: General Purpose, high luminosity detectors; Compact Muon Solenoid (CMS) [16] [17] and A Toroidal LHC Apparatus (ATLAS) [18] [19], fixed target detector for B physics: LHCb [20] and, ion detector: A Large Ion Collider Experiment (ALICE) [21].

### 3.2 The Compact Muon Solenoid Detector

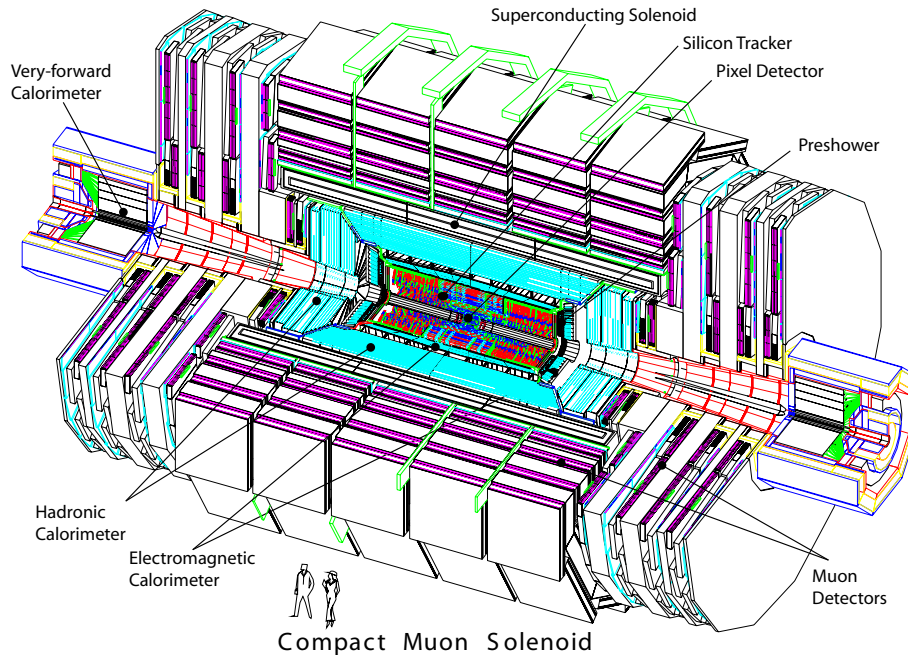


Figure 3.4: An overview of the CMS Detector [2]

CMS [2] [13] [16] [17] is one of two multi purpose apparatus located 100 m underground inside of experimental cavern at the Point 5 of CMS near to French village Cessy. 14 TeV designed energy implies 70 mb inelastic proton cross section and with the design luminosity of  $10^{27} \text{ cm}^{-2}\text{s}^{-1}$ ,  $7 * 10^7 \text{ Hz}$  interaction rate is expected and having 25 ns bunch crossing leads 1000 particles coming out of event of interest to be measured at the LHC collision points; the CMS and ATLAS detectors. This requires CMS to have low latency measurements and high granularity which are achieved by fast electronics and multi layered- multi channel detector structure. The CMS detector can also measure heavy ion collisions.

Clearly, as a particle detector main requirement for the CMS is to measure these interactions with high precision and speed. This requirement can be expanded as follow,

- Wide range covered, good muon identification and good dimuon mass resolution.
- Efficient online triggering and good momentum resolution and identification of charged

particles

→ Good diphoton, dielectric mass resolution; therefore, good electromagnetic resolution

→ Good dijet mass and missing-transverse-energy resolution

Physics goals can be listed as,

→ Measuring the SM to calibrate and understand the detector and further making precision measurements for the Standard Model.

→ Exploring TeV scale and testing possible Beyond the Standard Model predictions.

→ Understanding the origin of symmetry breaking and dark matter. → Understanding high energy Ion collisions and testing possible Beyond the Standard Model predictions.

The CMS detector has a multi layered structure which consists of different sub detectors each with a specific purpose.

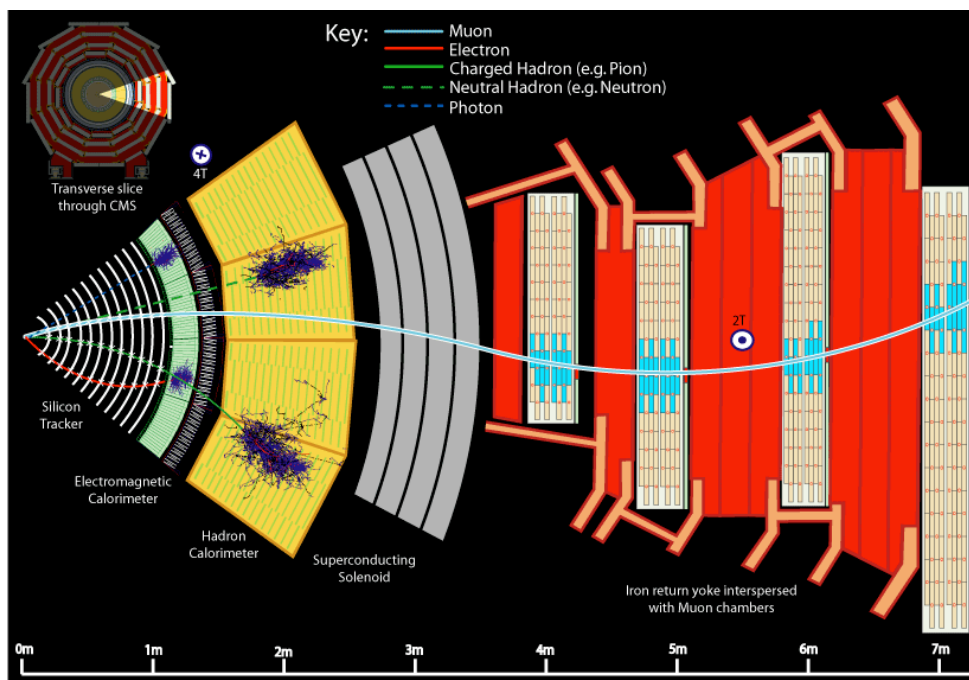


Figure 3.5: Layered Structure of CMS: Transverse Slice [22]

### 3.2.1 Inner Tracking System

With more than 200 m<sup>2</sup> of silicon surface (with 1440 pixel and 15148 strip detector modules), CMS tracker system [2] [13] [23] is the largest silicon tracker system ever built and consists of a -three barrel layers- pixel detector and a -ten barrel layers- silicon strip detector, which are closed by endcaps. The tracking system covers  $|\eta| < 2.5$ .

**Purpose of the detector:** Precise measurement of trajectory of charged particles and secondary vertex reconstruction.

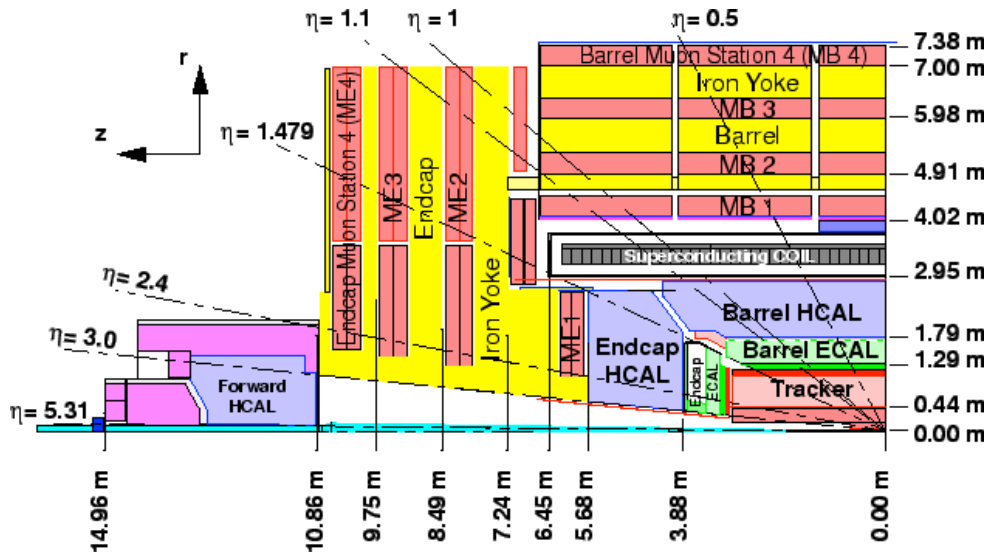


Figure 3.6: Layered Structure of CMS: Longitudinal Slice [24]

### 3.2.2 Electromagnetic Calorimeter (ECAL)

The Electromagnetic Calorimeter [2] [13] [25] is composed of 61200 lead tungstate (PbWO<sub>4</sub>) crystals placed in the barrel part completed by 7324 crystals in each of the two endcaps. Barrel (EB) covers a range of  $|\eta| < 1.479$ , while endcaps (EE) covers between  $1.479 < |\eta| < 3.0$  as it can be seen in figure 3.7.

**Purpose of the detector:** Identification of pions, electrons, photons, and position determination of electrons and photons.

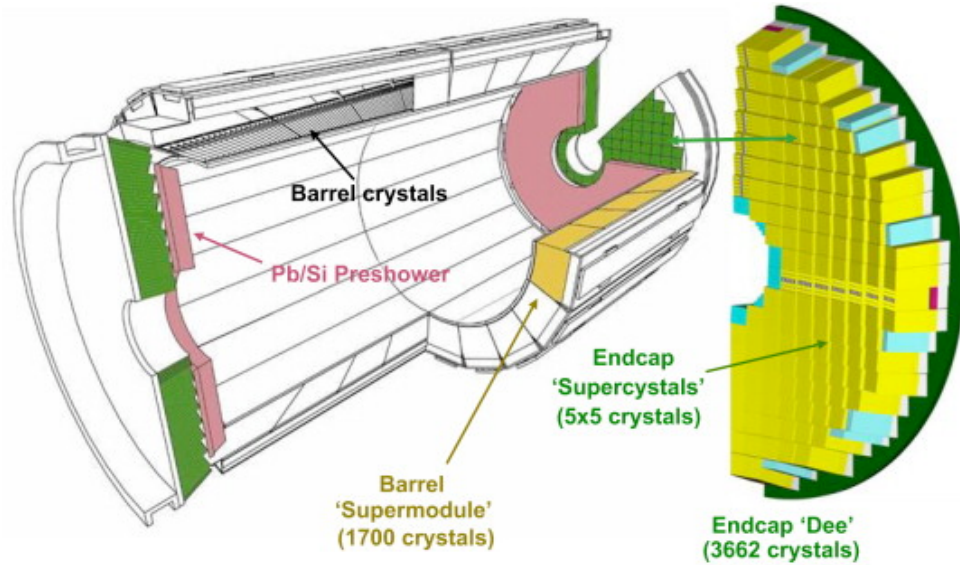


Figure 3.7: Overview of ECAL detector [26]

### 3.2.2.1 Photodetectors

There are two types of Photo-detectors for the Electromagnetic calorimeter, Avalanche photodiodes (APDs) in the barrel (central part) and vacuum phototriodes (VPTs) in the endcaps (two sides). These detectors are chosen and placed with respect to their radiation hardness.

### 3.2.2.2 Preshower

Preshower is placed in front of the ECAL endcaps and covers  $1.653 < |\eta| < 2.6$  region. It has two layers: Lead radiators to start electromagnetic showers and strip silicon detectors to measure energy.

### 3.2.3 Hadron Calorimeter

While it is radially placed between ECAL and Magnets, Hadron Calorimeter (HCAL) [2] [13] [27] covers  $|\eta| < 5.2$  with the forward hadron calorimeter. Structural design of HCAL can be divided into 4 parts: Barrel (HB), endcap (HB), outer calorimeter (HO), forward calorimeter (HF). **Purpose of the detector:** To measure hadron jets, neutrinos and new physics events related with missing transverse energy. HO has a supporting role which is to ensure precise

measurement hadrons while HE and HB struggle to control (late) hadron showers and HF is to take measurement at forward region of CMS  $3 < |\eta| < 5.2$ .

### **3.2.4 Forward Detectors**

Detection of particles at the very forward region of the CMS detector is maintained by CASTOR (CentauRO And Strange Object Research). CASTOR is composed of Quartz Tungsten plates which ensures the detector is working even in high radiation conditions. CASTOR covers  $5.2 < |\eta| < 6.6$  range.

### **3.2.5 The Muon System**

The muon system [2] [13] [28] is one of the most important elements that makes the CMS experiment so special as it can be deduced from its name. Muons are particles with usually higher energy and higher mass; therefore, are harder to detect and identify by a particle detector compared to electrons; however, muons are more significant for the search for new physics. The muon system is composed of four sub system:

#### **Drift Tube System**

The CMS barrel muon system is composed of 250 drift chambers placed in 4 concentric cylindrical layers. Drift Tube system takes care of electromagnetic cascades coming with muons and can be used as tracking detectors.

#### **Cathode Strip Chamber System**

There are 468 cathode strip chambers (CSC) aligned in CMS Endcap Muon system that covers an  $\eta$  range of 0.9 to 2.4. Built as multiwire proportional chambers, CSCs measure the radial position of muons.

#### **Resistive Plate Chamber System**

Resistive Plate Chambers provide a good spatial resolution and timing resolution for muon  $|\eta| < 1.6$  in a short time period (much less than  $< 25$  ns). This fast measuring time enables RPC for a fast dedicated muon trigger. It is designed as a parallel plate gaseous detector.

## **Optical Alignment System**

Due to constructional tolerances, magnetic field distortions and time dependent deformations, muon chambers and the central tracker in the CMS may be misaligned. However, a precise measurement of muons requires a flawless alignment of the order of  $\sim 100 \mu\text{m}$ . To achieve this, each sub system tracks mutual positions using optical alignment system and measurements are calibrated from the information gathered from optical alignment system.

### **3.2.6 Trigger and Data Acquisition**

The CMS detector has a data output rate of 40 MHz per bunch crossing (25 ns) [2] [13], which is nearly impossible to store with the existing technologies without doing any reduction. Therefore, two step triggering system is required to reduce data into a manageable size. The first step is Level-1 Trigger (L1) and the second level is High Level Trigger (HLT).

#### **3.2.6.1 Level-1 Trigger**

The aim of the CMS Level-1 Trigger [2] [13] system is to achieve fast data reduction and transfer data to higher trigger system with high reliability. This is accomplished by mostly sub detector specific systems. Level-1 Trigger is composed of electronics which allow to make fast decision thus data reduction. Two kinds of electronics are used for this purpose, ASICs (Application Specific Integrated Circuits) and FPGAs (Field Programmable Gate Arrays). ASICs are mainly radiation proof and designed for specific jobs hence more reliable and faster comparing to other solutions. However, since they are designed (and produced) for specific purposes, they are expensive to replace, upgrade or debug. On the other hand, FPGAs are more flexible and multi purpose. With the great leap forward in FPGA developments, in near future, FPGAs may become a better option over ASICs even in terms of performance and reliability. Currently, the CMS trigger and data acquisition systems use both FPGA and ASIC systems together, while ASICs are usually installed behind detectors itself and FPGAs are placed in control rooms close to detectors.

Each detector has its own local trigger:

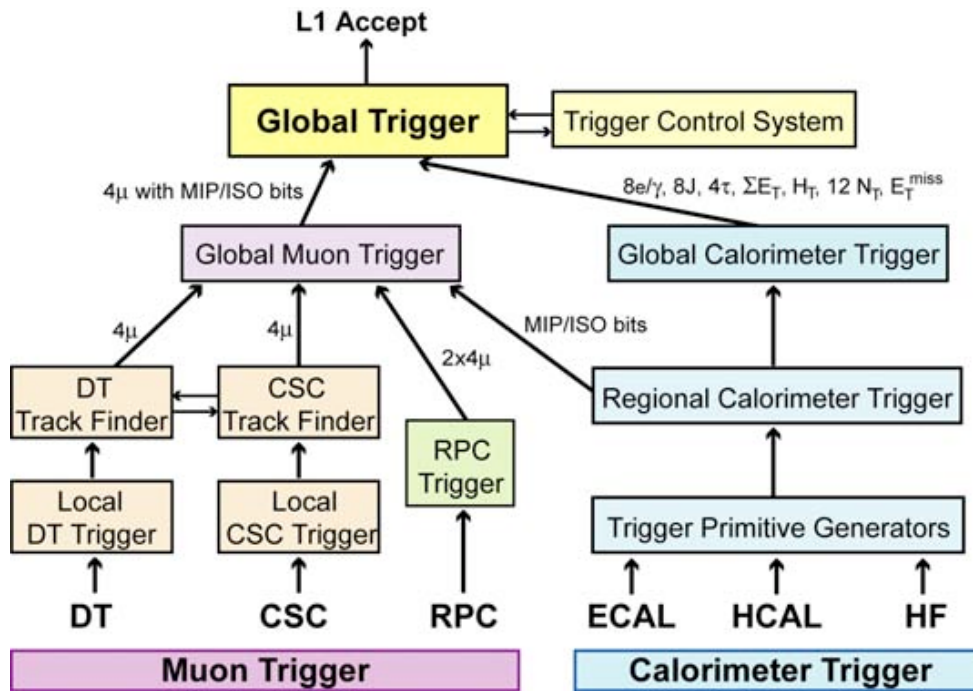


Figure 3.8: Triggering structure of the CMS experiment [2]

**Calorimeter Trigger:**

The Calorimeter Trigger uses the information measured in the ECAL and HCAL, and resolves the transverse energy, missing transverse energy, jets and jet counts. It also measures timing of the events (which should be same with bunch crossing) and synchronize data gathered from different calorimeters.

**Muon Trigger:**

The main purpose of this trigger is to match and connect different segments of the muon system and complete tracks of the muons. It also provides a good momentum and timing resolution of particles.

**Global Trigger:**

Global trigger has five level structure: Input, logic, decision, distribution and read-out. Global trigger decides whether event to be accepted or not using the information coming from sub detector trigger systems. After the decision, accepted events are sent to HLT with an output

rate  $\sim 30$  kHz (100 kHz max).

### 3.2.6.2 High Level Trigger and Data Acquisition

Main purpose of the HLT and Data Acquisition is to obtain further data reduction and event filtering. Event tagging has two main stages: reconstruct physics object and mark events having interesting features in terms of new physics. HLT requires to reach pace of L1 Trigger output thus requires massive parallelism with huge amount of computer power. The whole process of HLT is maintained by a computer farm with more than 9000 processor cores working at 2.6 GHz. The output of HLT is 200 Hz which corresponds  $\sim 350$  MB/s and with  $\sim 10^7$  seconds run per year CMS is expected to collect more than 3 PB of data per year.

### 3.2.7 Computing

Computing model [29] at the CMS experiment can be discussed under two main titles: Online and Offline computing. Since, offline computing structure is used in this analysis, offline computing will be mainly emphasized in this section.

#### 3.2.7.1 Offline Computing

Just like the detector, CMS Computing Model has a multi layered structure. Various Data formats are used in the CMS Computing Model and a data format can be simply defined as a C++ class in a computational point of view. Moreover, Data in the CMS computing model is divided into different *tiers*. Each of these tiers stands for different simulation or reconstruction step of the data. Type of data tiers and formats used in the CMS computing model can be listed as:

- **DAQ RAW** contains information collected from ASICs and FPGAs with L1 trigger results.
- **RAW** is composed of reduced data coming from computer farms and contains L1 and HLT selection informations. These informations are reconstructed by the event recon-

struction program.

- **RECO (Reconstructed Data)** contains information on reconstructed objects, hits and clusters. In order to reconstruct physics objects following procedure is followed
  1. Clusters are reconstructed and the detector acceptances are applied during unpacking and decoding of the detector data.
  2. Using hits in the silicon and muon detectors, particle tracks are reconstructed.
  3. Using different algorithms, standard particle definitions (used in physics analysis like electron, muon) are constructed.
- **AOD (Analysis Object Data)** is the reduced version of RECO data. It only includes information required for the physics analysis.
- **GEN** generated Monte Carlo events without any detector simulation.

Computing at the CMS has four hierarchic tier levels. The raw data are stored and distributed at Tier-0 placed in CERN. Also, first reconstruction steps are applied at this tier. Tier-1 operates the reconstruction, skimming and calibration steps and also provides a second secure copy to raw data. Finally, Tier-2 and Tier-3 provide local services and global grid distribution of the reconstructed data. Moreover, they operate the overall Monte Carlo sample generation for the experiment.

## CHAPTER 4

### DATA SELECTION AND MONTE CARLO SAMPLES

#### 4.1 Data Selection and Monte Carlo Samples

In the analysis of forward backward asymmetry, we used scattering angle distributions of the neutral bosons which are reconstructed from electron positron pairs. With this purpose, 2011 data collected by the CMS detector at 7 TeV LHC collisions is analyzed in this thesis. Data is chosen according to JSON (Java Script Object Notation) files which include good luminosity section information. For the high energy electrons, events used in the analysis should pass one of the *HLT\_DoublePhoton33*, *HLT\_DoubleEle33\_CaloIdL*, *HLT\_DoubleEle33\_CaloIdT* and *HLT\_DoubleEle45\_CaloIdL* triggers, which have a minimum  $E_T$  cut of 33 GeV, depending on their run numbers. The list of triggers with corresponding run intervals can be found in 4.1. Monte Carlo Samples for the Standard Model are generated via PYTHIA [30] and effects of

Table 4.1: Triggers and Corresponding run numbers used in  $A_{FB} - Z'$  analysis

Trigger	L1 Seed	Run Interval
HLT_DoublePhoton33	SingleEG20	160404-163869
HLT_DoubleEle33_CaloIdL	SingleEG20	165088-180252
HLT_DoubleEle33_CaloIdT	SingleEG20	178420-180252
HLT_DoubleEle45_CaloIdL	SingleEG20	178420-180252

the CMS detector are simulated via Geant4 [31]. The list of samples can be found in Table 4.2. MC samples for Sequential Standard Model are generated privately again via PYTHIA and Geant4 by using CMSSW interface. SSM  $Z'$  couplings are defined as usual SM couplings and mass of  $Z'$  is set to 1 TeV for this work. MC samples and Data can be compared in terms

of physics properties by normalizing MC with the normalization constant:

$$N_S = \int L dt \times \sigma \times \epsilon \quad (4.1)$$

where  $\epsilon$  is defined as the ratio of particles that passes through the cuts over total number of particles. To estimate errors, we use the formula  $\frac{1}{\sqrt{n}}$  where  $n$  is the number of entities in the corresponding histogram bin.

Table 4.2: MC Samples for SM and the corresponding cross sections.

Process	sample	generator	Cross Section (pb)	PDF set/tune
$DY \rightarrow e^+e^-$	DYToEE_M-20	Powheg	1666. (NNLO)	CT10 / Z2
	DYToEE_M-120	Powheg	10.3 (LO)	Z2
	DYToEE_M-200	Powheg	1.28 (LO)	Z2
	DYToEE_M-500	Powheg	0.0284 (LO)	Z2
	DYToEE_M-800	Powheg	0.00415 (LO)	Z2
$t\bar{t}$ like	DYToTauTau_M-20	Pythia	1666. (NNLO)	Z2
	$t\bar{t}$ Jets	Madgraph	163. (NNLO)	Z2
Jets	G_Pt-15to30	Pythia	171700. (LO)	Z2
	G_Pt-30to50	Pythia	16690. (LO)	Z2
	G_Pt-500to80	Pythia	2722. (LO)	Z2
	G_Pt-80to120	Pythia	442.2 (LO)	Z2
	G_Pt-120to170	Pythia	84.17 (LO)	Z2
	G_Pt-170to300	Pythia	22.64 (LO)	Z2
	G_Pt-300to470	Pythia	1.493 (LO)	Z2
	G_Pt-470o800	Pythia	0.1323 (LO)	Z2
	WJetsToLNu	madgraph	31.314 (NLO)	Z2
	WJetsToLNu_PtW100	madgraph	260. (NLO)	Z2

## 4.2 Electron Reconstruction

First step of the electron construction [32] [33] is to reconstruct ECAL clusters. In order to do that two different algorithms are used: Hybrid algorithm for barrel and multi5x5 algorithm for endcaps. The strategy is to collect energy coming from showering due to bremsstrahlung of electrons in a cone around seed crystal of 0.3 rad. After that, to select trajectory seeds, hits in the innermost tracker layers are matched with superclusters. Matching process uses energy weighted average impact point of the electron and photons coming from the bremsstrahlung of the electrons, to ensure these particles coming from interaction. This method is especially efficient for high  $p_T$  electrons. Then to construct trajectories of electrons all electron seeds are used and electron track parameters are estimated using a Gaussian Sum Filter (GSF) fit.

The final step is the estimation of the true fraction of energy by taking the difference between the momentum at the outermost track position and innermost track position. All information gathered in these steps is put into GsfElectron object which can be accessed via CMSSW.

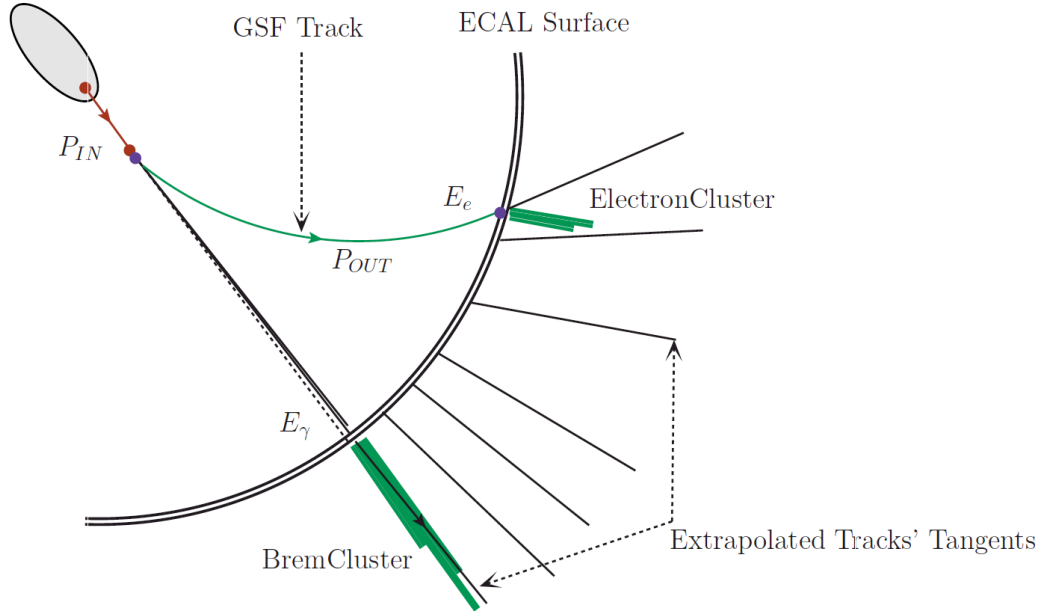


Figure 4.1: GSF Electron interaction with the detector

In order to subtract irrelevant events (backgrounds, mis-identified particles, etc) identification cuts are applied to the reconstructed particles. These selection criteria are composed of cuts on different variables that describes the electron object. High Energy Electron Pairs (HEEP) selection criteria are used in this analysis. A summary of HEEP selection criteria can be found in Table 4.3. HEEP Selection criteria are separated into two sets with respect to pseudo rapidity distribution of Electromagnetic Calorimeter sections:  $|\eta| < 1.442$  corresponds to the Barrel Electromagnetic Calorimeter region and  $2.5 > |\eta| > 1.560$  corresponds to the Endcap Electromagnetic Calorimeter region (EE).  $E_T$  of the electrons should be higher than 35 GeV in the barrel region (EB), and higher than 40 GeV in end cap, where  $E_T$  can be defined as multiplication of sine of polar angle of electron track interpolated to the vertex and super cluster energy.

Definitions of selection cuts [34] [35] are given below ,

- $\eta_{SC}$  → Defined as pseudorapidity of the supercluster of electron.
- $\Delta\eta_{in}$  → Defined as the alignment differences of track position measurements at inner layer, interaction vertex, calorimeter and supercluster in  $\eta$  plane.
- $\Delta\phi_{in}$  → Defined as the alignment differences of track position measurements at inner layer, interaction vertex, calorimeter and supercluster in  $\phi$  plane.
- $H/E$  → Defined as the ratio of the hadronic energy Calorimetry Towers within a cone  $\Delta R < 0.15$  in the HCAL and supercluster energy of electron candidate.
- *ECAL Isolation* → Defined as the transverse EM energy of all the reconstructed hits with  $|E| > 0.08$  GeV ( $|E_T| > 0.1$  GeV endcap) in a cone of  $\Delta R < 0.3$  centered on the electron's position in the calorimeter. However, those in an inner cone of radius 3 crystals and eta strip of total width of 3 crystals are excluded. To exclude these crystals, their positions have to be defined. Since the crystal width approximately corresponds to a value in  $\eta$  plane, by putting an  $\eta$  cut these effects can be removed. Corresponding values are 0.0174 in the barrel and  $0.00864 * |\sinh \eta|$  in endcap. This variable is used only in a sum with the hadronic depth 1 isolation defined below.
- *Hadronic Depth1 Isolation* Defined as the transverse depth 1 hadronic energy of all the HCAL Calorimetry Towers in a cone of  $\Delta R < 0.3$  centered on the electron's position in the calorimeter, excluding Calorimetry Towers in a cone of  $\Delta R < 0.15$ . Depth 1 is defined as All depths Towers 1-17, depth 1 Towers 18-29, depth 2 Towers 27-29.
- *Track  $P_T$  Isolation* → It is defined as the sum  $p_T$  of the tracks in a deltaR cone of 0.04-0.3 with  $P_T > 0.7$  GeV/c and z0 with  $\pm 0.2$  of the z0 of the electrons GsfTrack and  $d0 < 9999$ . The variable z0 is minimum distance in z from the point 0,0,0. The variable d0 is the minimum distance in the x,y plane from the beamspot.

Also, since particle flow is not acceptable for high energy electrons, Ecal driven electrons are chosen [34]. All electron pairs that pass through HEEP selection also pass online trigger. Therefore, no additional restrictions are applied to the Monte Carlo simulations.

Table 4.3: HEEP Selection Criteria: While first two variables stand for kinematic and geometric properties, second set stands for identification (ID) cuts and third set for the isolation cuts.

Selection Variable	EB	EE
$E_T$	$> 35 \text{ GeV}$	$> 40 \text{ GeV}$
$ \eta_{SC} $	$< 1.442$	$1.56 <  \eta_{SC}  < 2.5$
MH in Inner Pixel	$= 0$	$= 0$
$ \Delta\eta_{in} $	$< 0.005$	$< 0.007$
$ \Delta\phi_{in} $	$< 0.09$	$< 0.09$
$H/E$	$< 0.05$	$< 0.05$
$E^{2\times 5}/E^{5\times 5}$	$> 0.94$	-
or		
$E^{1\times 5}/E^{5\times 5}$	$> 0.83$	-
isol Em + Had Depth 1	$< 2 + 0.03 \times E_T \text{ GeV}$	$< 2.5 \text{ GeV}$ for $E_T < 50 \text{ GeV}$ : $< 2.5$ $+0.03 \times (E_T - 50) \text{ GeV}$
isol Pt Tracks	$< 7.5 \text{ GeV}/c$	$< 15 \text{ GeV}/c$

### 4.3 Z Boson Reconstruction

Two highest  $p_T$  electrons that pass HEEP selection criteria with opposite charges are selected to reconstruct neutral bosons that mediate  $q\bar{q} \rightarrow e^-e^+$  interaction.

Table 4.4: Fraction of particles that pass through HEEP Selection Criteria in percentage. Here the column headers give the name of corresponding data and MC samples.

Selection Variable	May10th	Aug5th	APromptv6	BPromptv1	DYtoEE20
$E_T$	79.5	81.2	81.6	81.57	85.6
$ \eta_{SC} $	97.4	97.3	97.4	97.4	97.0
MH in Inner Pixel	97.4	92.5	92.5	92.7	98.3
$ \Delta\eta_{in} $	47.4	50.0	50.4	52.2	92.3
$ \Delta\phi_{in} $	66.3	67.7	68.0	69.0	93.6
$H/E$	55.8	59.0	59.6	61.0	94.1
$E^{2\times5}/E^{5\times5}$	49.8	52.4	52.6	61	92.8
isol Em + Had Depth 1	20.4	23.6	23.8	24.0	86.8
isol Pt Tracks	32.7	36.6	37.1	40.1	94.9

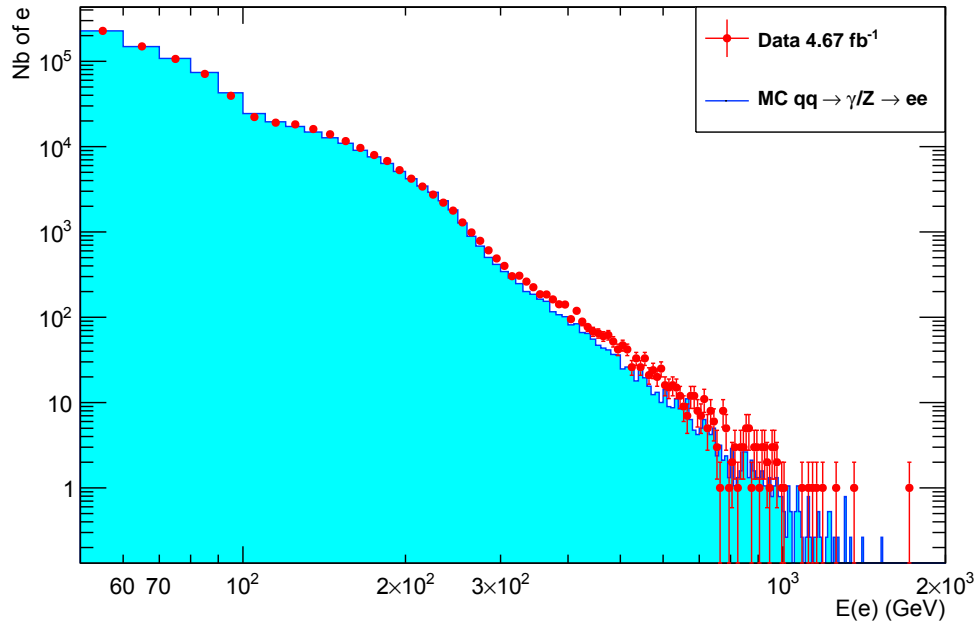


Figure 4.2: Energy distribution of opposite charged dielectron pairs

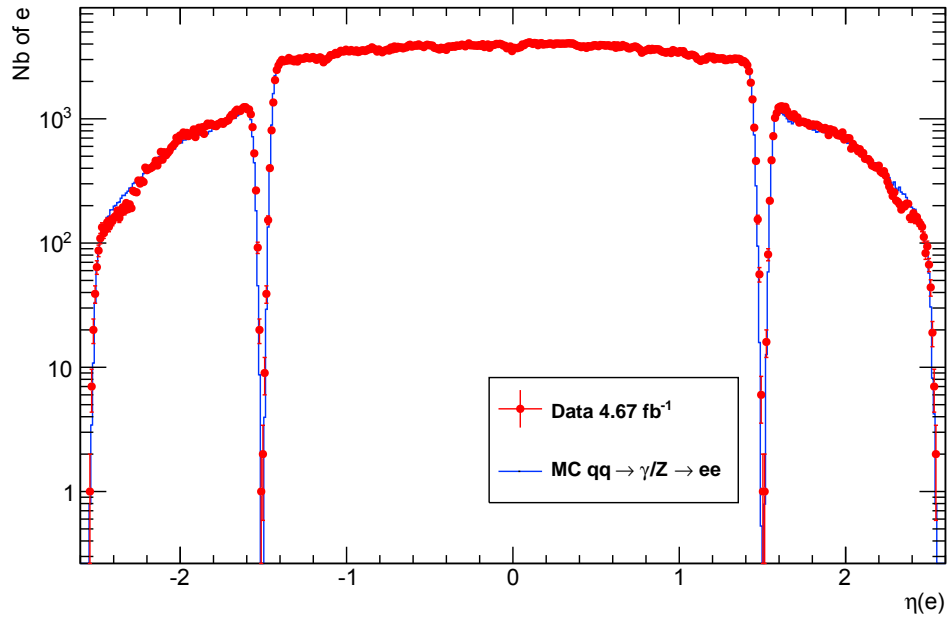


Figure 4.3: Pseudo rapidity distribution of oppositely charged dielectron pairs

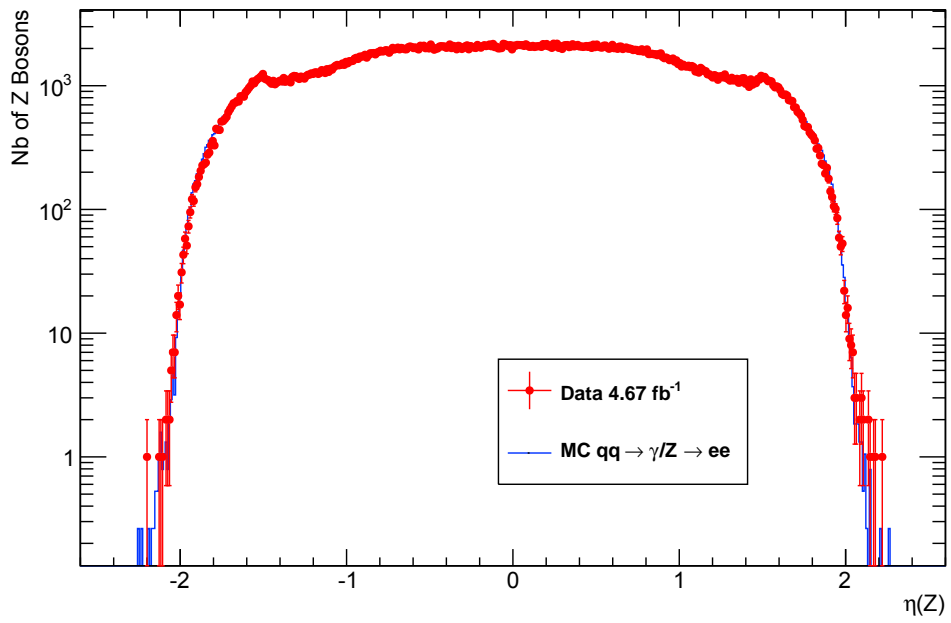


Figure 4.4: Pseudo rapidity distribution of reconstructed Z bosons

Differences between MC samples and Data can be accounted to Standard Model (SM) backgrounds (electron pairs created from other SM processes). However,  $q\bar{q} \rightarrow Z \rightarrow e^-e^+$  should dominate near  $Z^0$  pole ( $\sqrt{s} \sim 91$  GeV). Hence, incompatibility at this mass region can not be accounted to the SM backgrounds. The problem arises from the fact that Detector simulations on MC samples does not hundred percent reflect of real world scenario. Therefore these additional corrections should be applied to externally by hand. To do that, energy measurements in the data should be scaled to a factor which can be obtained by finding the shift of the  $Z^0$  peak from the accepted  $Z^0$  mass (from the Particle Data Group [36]).

To do that, Crystal-Ball fit is applied to both data and Monte Carlo samples and difference between apparent and accepted mass of  $Z^0$  ( $\Delta m_{CB}$ ) is obtained, finally scaling factor is defined as  $\frac{\Delta m_{CB}(data) - \Delta m_{CB}(MC)}{m(Z^0)}$ .

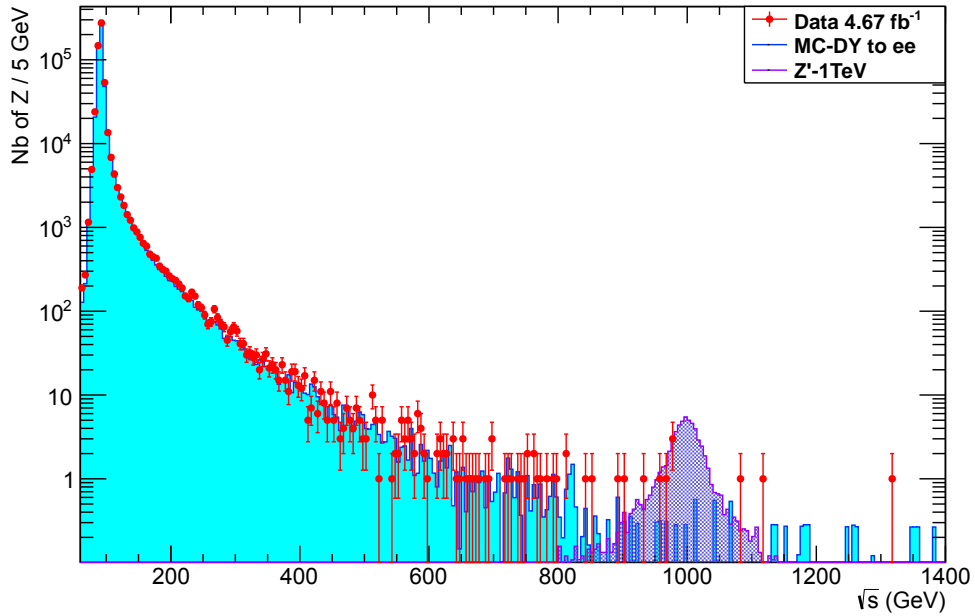


Figure 4.5: Invariant Mass histogram in range: 0.06-1.4 TeV

## CHAPTER 5

### ANALYSIS OF FORWARD BACKWARD ASYMMETRY

In this section, results obtained from  $A_{FB}$  analysis and possibility for  $Z'$  particle searches via  $A_{FB}$  will be discussed. Angular distribution of dielectrons and additional effects in angular distribution will be discussed in first part, after that results will be presented, finally errors and background subtraction will be discussed.

#### 5.1 Scattering Angle Distributions in the Collins Soper Frame

Even after the Collins Soper frame is picked as the Center of Mass frame and forward direction is corrected with respect to valance quark, there are still additional issues on angular momentum of leptons, hence on forward backward asymmetry. These disturbances are related to

- QED Final State Radiation (FSR): Although it is not as effective as initial state radiation, it changes the lepton momentum depending on the energy released of bremsstrahlung process. QED FSR is especially effective near Z boson peak.
- Acceptance of CMS Detector: The CMS detector, in design, covers more than 5 in eta plane (which covers almost entire solid angle), however, to get precise measurements of electrons Electromagnetic Calorimeter is required which covers only  $|\eta| < 2.5$ .

All of these effects above cause a change in a shape of  $\cos \theta_{CS}^*$  and bin migration which result with the dilution of asymmetry. Fluctuations arise from QED FSR and finite resolution can be reversed by unfolding data to born level. Unfolding [38] is mainly necessary for

- merging results gathered from different physics conditions (for example different final states,  $Z/\gamma^* \rightarrow e^-e^+$  and  $Z/\gamma^* \rightarrow \mu^-\mu^+$ )
- comparing the results with an outdated experiment
- reverse unintended effects to compare data with ground theory.

On the other hand, comparison can be made without unfolding the data because the additional effects can also be applied to theoretical expectations. Therefore, for our discussion we use Monte Carlo samples in which these effects have already been simulated (more detailed discussion on unfolding and application on  $A_{FB}$  can be found in the analysis [37]). That means results discussed here will be uncorrected (un-unfolded).

Here uncorrected  $\cos \theta_{CS}^*$  distributions for different mass bins (mass intervals) are presented in order to have a better understanding of distributions in high invariant mass and low invariant mass regions. First figure 5.1 shows  $\cos \theta_{CS}^*$  in low mass region and second figure 5.2 gives high energy case. Fluctuations observed in second graph is the natural result of lack of statistics. However, still the symmetric distribution of  $Z'$  can be observed while MC and Data distributions display the asymmetry in forward direction as expected.

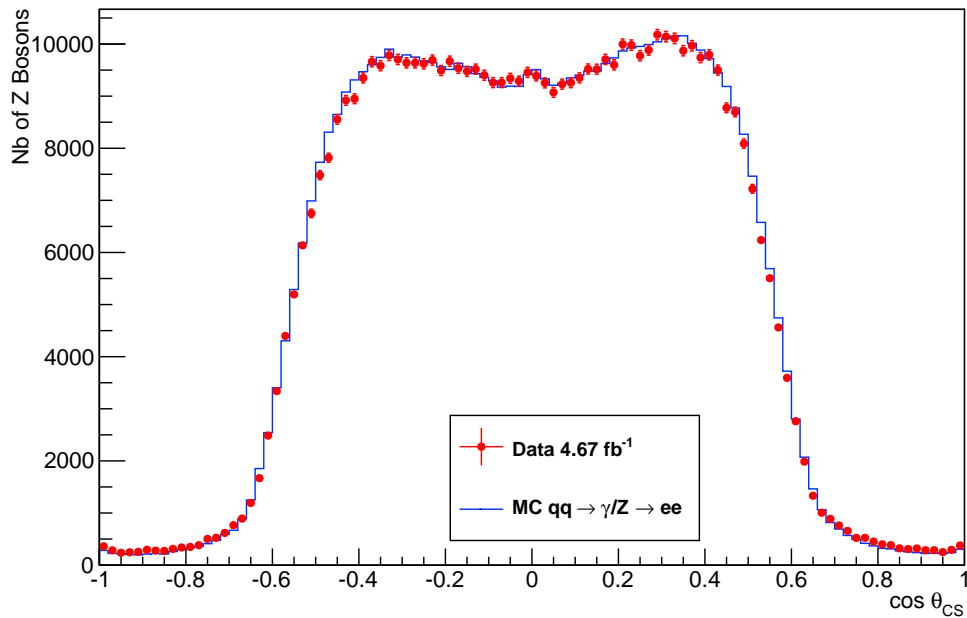


Figure 5.1:  $\cos \theta_{CS}^*$  distribution within an invariant mass interval of  $60\text{GeV} < \sqrt{s} < 300\text{GeV}$ .

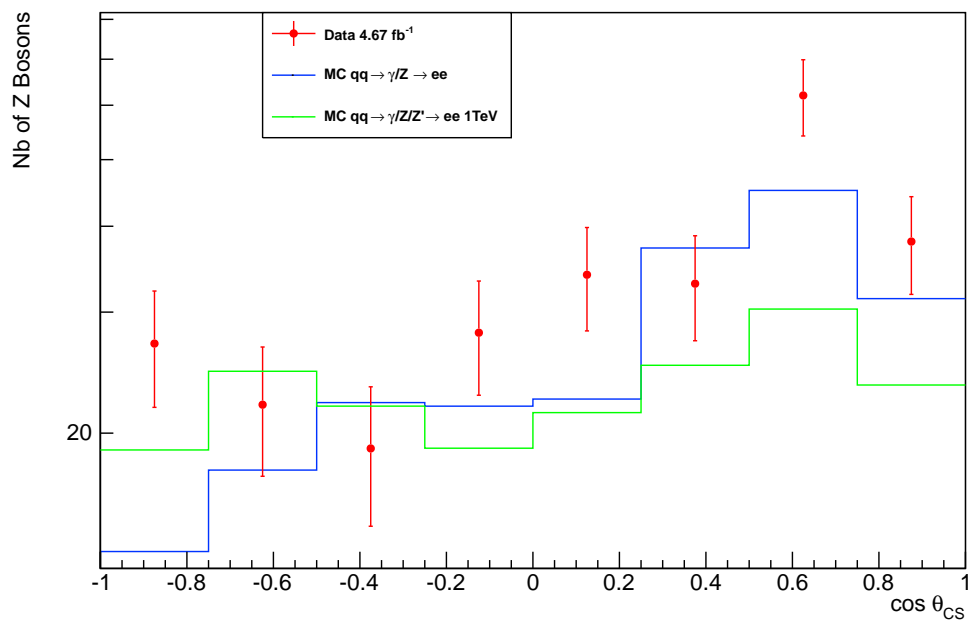


Figure 5.2:  $\cos\theta_{CS}^*$  distribution within an invariant mass interval of  $400\text{GeV} < \sqrt{s} < 1400\text{GeV}$

## 5.2 Forward Backward Asymmetry

We defined Forward Backward Asymmetry earlier,

$$A_{FB} = \frac{F - B}{F + B} = \frac{3A_1}{8A_0} \quad (5.1)$$

Since we have already applied boost effect,  $F$  ( $B$ ) can be given as particle going in  $\cos \theta_{CS}^* > 0$  ( $0 > \cos \theta_{CS}^*$ ) respectively. We separate our energy scale into a set of invariant mass bins (60-76, 76-86, 86-96, 96-106, 106-120, 120-150, 150-200, 200-300, 300-500, 500-750, 750-1400 GeV) and for each invariant mass bin, mean values of bin contents are found to place data points. Further, to have better understanding of the detector and QED FSR effects,  $A_{FB}$  graphs will be discussed in 3 different rapidity regions:  $0.8 > |Y| > 0$ ,  $2.5 > |Y| > 0.8$  and  $2.1 > |Y| > 0.8$ . Errors in the  $A_{FB}$  plots are calculated using the following equation,

$$\Delta A_{FB} = \sqrt{\frac{1 - A_{FB}}{N}} \quad (5.2)$$

where  $N$  is the total number of event content in the bin.

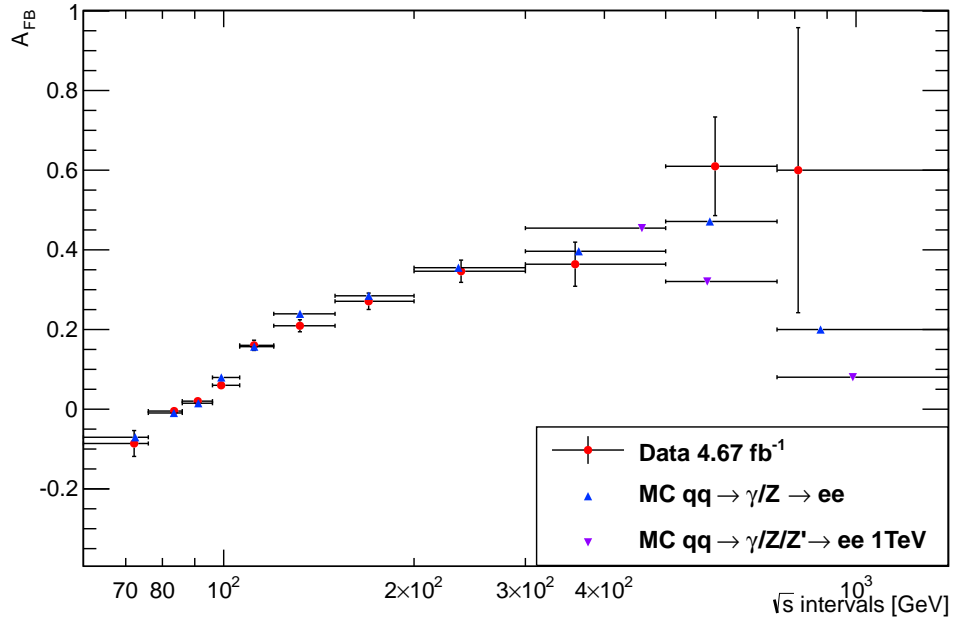


Figure 5.3: Forward Backward Asymmetry within the range  $2.5 > |Y| > 0.8$  and  $60\text{GeV} < \sqrt{s} < 1400\text{GeV}$

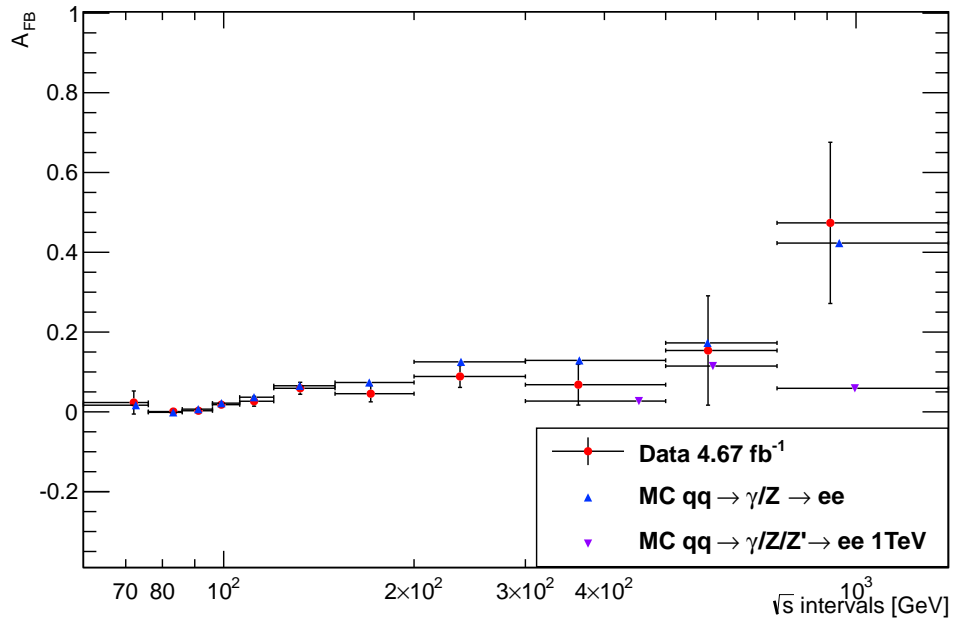


Figure 5.4: Forward Backward Asymmetry within the range  $0.8 > |Y|$  and  $60\text{GeV} < \sqrt{s} < 1400\text{GeV}$

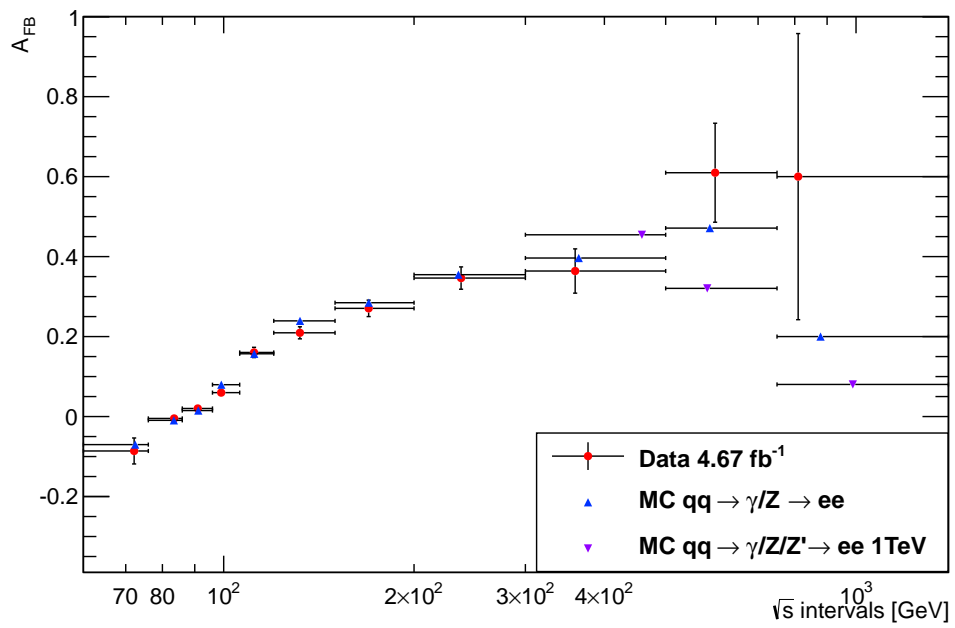


Figure 5.5: Forward Backward Asymmetry within the range  $2.1 > |Y| > 0.8$  and  $60\text{GeV} < \sqrt{s} < 1400\text{GeV}$

Figure 5.3 clearly shows the effects of both initial and final state radiations. To have a better understanding in this situation, boost effects that we have discussed in section 2 should be considered. In a low momentum and high momentum particle collision, resulting particle (since we have one resulting particle:  $Z$  or  $\gamma$  boson) follows the direction of the initial particle with higher momentum. Initial photon, gluons may boost quarks in transverse direction. Therefore, the  $Z$  particles in low rapidities are either created by these boosted quarks or reconstructed from misleading electrons that are boosted in an arbitrary direction via QED FSR. In both cases, since information of initial quarks' directions are lost, we could not obtain healthy  $A_{FB}$  measurements. Therefore, all of the bins give very small contributions to forward backward asymmetry except the highest invariant mass bin where statistics is very low so that results tend to fluctuate easily. Figure 5.4 on the other hand displays a better picture of Forward Backward Asymmetry between  $\sim 90\text{GeV} < \sqrt{s} < \sim 750\text{GeV}$ , though loss of statistics dramatically high in high invariant mass bins, other mass bins are close to the theoretical picture described in chapter 2. Finally, in figure 5.5 by applying tighter rapidity cut, we try to get a better result of  $A_{FB}$ . With these results we also show that in spite of its benefits, a rapidity cut decreases the statistics in high invariant mass region, hence it will not be useful for the purpose of this analysis.

We can discuss roughly the existence of  $Z'$  boson in figure 5.6. The differences between Data and  $Z'$  Monte Carlo sample can be seen even without a detailed statistical discussion at high invariant mass bins. However, to put a mass limit on existence of  $Z'$  boson requires a multi dimensional statistical analysis on  $A_{FB}$  and on invariant mass.

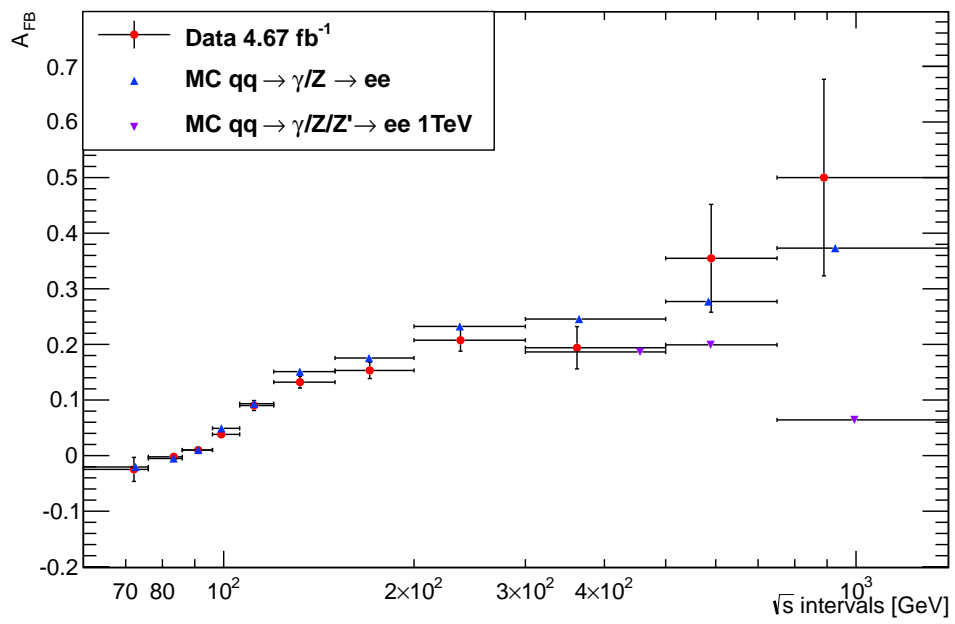


Figure 5.6: Forward Backward Asymmetry within the range  $60\text{GeV} < \sqrt{s} < 1400\text{GeV}$

## CHAPTER 6

### CONCLUSION

In this thesis,  $4.67 \text{ fb}^{-1}$  2011 CMS data is used to analyze the forward backward asymmetry. The forward backward asymmetry is not only an ideal tool to obtain precise measurements of the standard model interactions but also a good way to test possible theories beyond the standard model, since majority of these theories propose new neutral gauge bosons. On the other hand, it is yet another great challenge for the experimental physicists at the LHC due to the fact that measuring a quantity that depends on angular distributions so sensitively is very difficult in extremely populated proton collisions. In this analysis, we have discussed the effects of heavy neutral gauge bosons as well as the additional factors that negatively effect experimental measurements on the forward backward asymmetry.

The factors that dilute the shape of the forward backward asymmetry are

- Gluon and photon emissions of quarks
- Photon emission of dileptons
- Detector acceptance and limited resolution

First two effects are the result of different bremsstrahlung processes while the last one is directly related to the performance of the CMS detector. These factors dilute the asymmetry, hence they have a great negative effect on the forward backward asymmetry analysis.

The important conclusions obtained from the analysis can be summarized as follows:

- Forward backward asymmetry can be used as a  $Z'$  discovery tool, and it can give better

results than other methods for  $Z'$  models with large invariant mass width.

- Effects of final photon emission of dileptons and initial bremsstrahlung, even in the Collins Soper frame, cause dilution in low rapidities. Therefore, higher rapidities give better results in terms of forward backward asymmetry however with low statistics.
- More data is required to make an efficient statistical analysis of the forward backward asymmetry.

## REFERENCES

- [1] L. Evans and P. Bryant *LHC Machine*, JINST **3** S08001 (2008).
- [2] The CMS Collaboration, *The CMS Experiment at the CERN LHC*, JINST **3** S08004 (2008).
- [3] F. Halzen and A. Martin , *Quarks and Leptons*, Wiley (1984).
- [4] The LEP Electroweak Working Group and the SLD Electroweak and Heavy Flavour Groups, Phys. Rept. 427 (2006) 257.
- [5] J.C. Collins, D.E. Soper, Phys. Rev. D **16**, 2219 (1977).
- [6] M. Dittmar, A. Nicollerat, A. Djouadi *Phys. Lett. B* **584** (2004) 111-120.
- [7] P. Langacker, R. W. Robinett and J.L. Rosner 1984 *Phys. Rev. D* **30** 1470.
- [8] D. London and J.L. Rosner 1986 *Phys. Rev. D* **34** 1530.
- [9] J.L. Rosner 1987 *Phys. Rev. D* **35** 2244.
- [10] M. Cvetič and S. Godfrey 1995 *Electroweak Symmetry Breaking and New Physics at the TeV scale* Barklow T L (ed.) et al (World Scientific) p 383; *Preprint* hep-ph/9504216
- [11] J. Rosner , *Phys. Rev. D* **54**, 1078 (1996).
- [12] Scheme of the LHC, [http://doc.cern.ch/archive/electronic/cern/others/PHO/photo-ac/9906026\\_01.jpe](http://doc.cern.ch/archive/electronic/cern/others/PHO/photo-ac/9906026_01.jpe), Last accessed 16.03.2012.
- [13] D. Green (ed), *At the Leading Edge: The ATLAS and CMS LHC Experiments*, World Scientific (2010).
- [14] LHC schematics, <http://public.web.cern.ch/public/en/research/AccelComplex-en.html>, Last accessed 16.03.2012.
- [15] Dipoles at the LHC, [http://images.iop.org/objects/ccr/cern/46/8/19/CCEthe1\\_10-06.giff](http://images.iop.org/objects/ccr/cern/46/8/19/CCEthe1_10-06.giff), Last accessed 16.03.2012.
- [16] CMS Collaboration, *CMS Technical Design Report Vol. I: Detector Performance and Software*, CERN/LHCC 2006-001 (2006).
- [17] CMS Collaboration, *CMS Technical Design Report, Vol. II: Physics Performance*, J. Phys. G., vol. **34**, number 6 (2007).
- [18] The ATLAS Collaboration, *ATLAS Detector and Physics Performance Technical Design Report  $\checkmark$  Vol. I*, (1999), CERN/LHCC 99-14.
- [19] The ATLAS Collaboration, *ATLAS Detector and Physics Performance Technical Design Report  $\checkmark$  Vol. II*, (1999), CERN/LHCC 99-15.

- [20] The LHCb Collaboration, *LHCb: Technical Proposal*, CERN, Geneva, (1998), CERN/LHCC 98-004.
- [21] The ALICE Collaboration, *Technical Design Report*, (Oct, 2001), CERN/LHCC 2001-021.
- [22] Transverse Slice of the CMS Detector, [http://mkirsano.web.cern.ch/mkirsano/Slice\\_black\\_lores.gif](http://mkirsano.web.cern.ch/mkirsano/Slice_black_lores.gif), Last accessed 16.03.2012.
- [23] The CMS collaboration, *The CMS Tracker System Project: Technical Design Report*, CERN-LHCC-98-006 (1998).
- [24] Longitudinal Slice of the CMS Detector, <http://www.hephy.at/user/friedl/diss/html/img41.gif>, Last accessed 16.03.2012.
- [25] The CMS collaboration, *The Electromagnetic Calorimeter Project: Technical Design Report*, CERN-LHCC-97-033 (1997).
- [26] ECAL, <http://www.sciencedirect.com/science/article/pii/S0168900211005572> 16.03.2012.
- [27] The CMS collaboration, *The Hadron Calorimeter Project: Technical Design Report*, CERN-LHCC-97-031 (1997).
- [28] The CMS collaboration, *The CMS muon project, Technical Design Report*, CERN-LHCC-97-032 (1997).
- [29] Computing model of the CMS experiment, <https://twiki.cern.ch/twiki/bin/view/CMSPublic/WorkBookComputingModel>, Last accessed 24.03.2012.
- [30] T. Sjostrand, S. Mrenna, and P. Z. Skands, *PYTHIA 6.4 Physics and Manual*, JHEP **05** (2006) 026.
- [31] J. Allison et al., *Geant4 Developments and Applications*, IEEE Trans. Nucl. Sci. **53** (2006) 270.
- [32] The CMS Collaboration, *Electromagnetic physics objects commissioning with first LHC data*, CMS PAS EGM-2010/001 (2010).
- [33] S. Baf̄soni et al., *Electron reconstruction in CMS*, Eur. Phys. J. C **49** (2007), no. 3, 1099.
- [34] More information about HEEP: <https://twiki.cern.ch/twiki/bin/view/CMS/HEEPElectro nID>, Last accessed 16.03.2012.
- [35] B. Clerbaux, D. Cockerill, G. De Lentdecker, V. Dero, Sh. Elgammal, A. Gay, S. Harper, T. Hreus, G. Kukartsev, Ph. Mine, E. Olaiya, D. Petyt, T. Reis, C. Shepherd-Themistocleous, L. Thomas, V. Timciuc, and P. Vanlaer, CMS AN-Note 2011/ 159 (2011).
- [36] K. Nakamura et al. (Particle Data Group), J. Phys. G **37**, 075021 (2010).
- [37] The CMS Collaboration, CMS PAS EWK-11-004 (2011).
- [38] G. Cowan, *Statistical Data Analysis*, Oxford Press (1998).